Identifying mechanisms of resistance to oncolytic virotherapy in acute leukemia through a genome-wide CRISPR screen

by

Elaine Rose

A thesis submitted in partial fulfillment of the requirements for the degree of Master of Science in Biochemistry

University of Ottawa

Faculty of Medicine

July 23, 2018

Supervisors: Dr. John Bell and Dr. Natasha Kekre

Abstract

Approximately half of all adults diagnosed with acute leukemia (AL) relapse after standard chemotherapy, highlighting the need for alternative treatment options. We have previously shown that vaccination with irradiated autologous tumour cells infected with an oncolytic virus (OV) can elicit a durable, tumour specific, T cell-mediated response in a mouse model of AL. In the context of this AL infected cell vaccine (ICV) model, infection of autologous cells *ex vivo* with an OV is essential for stimulating a lasting immune response. While the murine AL line L1210 can be robustly infected with Maraba MG1, creating a potent infected cell culture, this ICV still has room for improvement as ICV-vaccinated mice with high tumour burden still die from leukemia. Therefore, we sought to utilize a genome wide CRISPR-Cas9 screen to identify genetic factors that mediate OV resistance in this model of AL. L1210 cells stably expressing Cas9 were transduced with the mouse GeCKOv2 library, which contains 130,209 gRNAs against 20,611 genes within the mouse genome. Following selection, cells were treated with Maraba MG1 and genomic DNA from resistant populations was sequenced to identify genes enriched in resistant cells relative to mock treated cells. Our screen identified several genes that mediate susceptibility to OV infection including those involved in viral entry (*Ldlr*), receptor-mediated endocytosis (*Atp6v1g2*), intracellular signaling (*Cav1*), the cytoskeleton (*Filip1* and *Tmod4*), as well as autophagy and exosome production (*Atg5*). We aim to use the findings from this work to improve therapeutic efficacy in otherwise OV resistant tumour models as well as identify biomarkers, to determine the feasibility of administering an ICV using patient derived tumour cells.

Acknowledgements

I would like to acknowledge and thank my co-supervisors John Bell and Natasha Kekre for their valuable guidance and support throughout my degree and beyond. Thank you to Larissa Pikor for patiently teaching me everything I now know about CRISPR and discussing many ideas together. I would like to thank Julia Petryk and Christiano De Souza for their assistance with animal injections and handling. Thank you to the many members of the 3rd floor Cancer Center at the OHRI for their friendship, advice and encouragement. Finally, I would like to thank my family for their never-ending love and support.

Table of Contents

List of Abbreviations

Adam10: A disintegrin and metalloprotease 10
AL: Acute leukemia
ALL: Acute lymphoblastic leukemia
Allo: Allogeneic
Atf3: Activating transcription factor 3
Atg: Autophagy protein
BCG: Bacillus calmette–guerin
CAR T cell: Chimeric antigen receptor T cell
Cas9: CRISPR-associated protein 9
Cav1: Caveolin-1
CR: Complete remission
CREB: cAMP responsive element-binding
CRISPR: Clustered regularly interspaced short palindromic repeats
CTLA-4: Cytotoxic T lymphocyte antigen 4
DC: Dendritic cell
DMEM: Dulbecco's modified eagle medium
DNA: Deoxyribonucleic acid
DSB: Double strand break
eIF2A: Eukaryotic translation initiation factor 2
ER: Endoplasmic reticulum
FBS: Fetal Bovine Serum
FDR: False discovery rate
Filip: Filamin-A interacting protein
GeCKO: Genome-wide CRISPR knockout
GFP: Green fluorescent protein
gRNA: Guide RNA
HIV: Human immunodeficiency virus
HR: Homologous recombination
HSCT: Hematopoietic stem cell transplant
ICV: Infected cell vaccine
IFN: Interferon
IRF: Interferon regulatory factor
ISG: Interferon stimulated gene
IV: Intravenous
JAK: Janus kinase
KO: Knockout
LDL: Low density lipoprotein
LDL-R: Low density lipoprotein receptor
MG1: Maraba mutated virus
MHC: Major histocompatibility complex
MOI: Multiplicity of infection
MRD: Minimal residual disease
NCS: Newborn calf serum
NDV: Newcastle disease virus

NF-κB: Nuclear factor kappa-light-chain-enhancer of activated B cells
NHEJ: Non-homologous end joining
OV: Oncolytic virus
PAM: Protospacer adjacent motif
PBS: Phosphate-buffered saline
PCR: Polymerase chain reaction
PD-1: Programmed cell death 1
Ph: Philadelphia chromosome
PKR: RNA-dependent protein kinase
RPM: Reads per million
STAT: Signal transducer and activator of transcription
SQ: Subcutaneous
TKI: Tyrosine kinase inhibitor
TLR: Toll-like receptor
Tspan: Tetraspanin
V-ATPase: Vacuolar ATPase
VSV: Vesicular stomatitis virus

List of Figures

List of Tables

Chapter 1: Introduction

1.1 Leukemia

1.1.1 Acute lymphoblastic leukemia

Leukemia is a blood cancer mostly caused by the uncontrolled proliferation of immature blood cells. Approximately 6000 Canadians were diagnosed with acute leukemia (AL) and 2900 died in 2017[1]. AL typically progresses quickly without treatment, and patients often succumb to the disease. The hematopoietic stem cell lineage consists of multipotent stem cells present in bone marrow that differentiate into common myeloid or lymphoid progenitors and as a result, AL is further classified by the cell lineage that is affected. Acute lymphoblastic leukemia (ALL) is the most commonly diagnosed pediatric cancer, comprising 32% of all cancer diagnoses in children 0-14 years old between 2006-2010[1], and generally follows a bimodal distribution, affecting children and older adults most often[2,3]. ALL is comprised of lymphoblast cells that no longer differentiate into T or B lymphocytes, but instead proliferate abnormally. Diagnosis by blast cell percentage is typically confirmed by a complete blood count as well as laboratory sample testing from peripheral blood and bone marrow biopsy[4]. ALL patients may suffer a number of problems caused by their unforgiving disease. The aggressive nature of the cancer leads to significant pancytopenia and bleeding from thrombocytopenia, anemic symptoms and infections related to neutropenia, all caused by low blood counts due to bone marrow infiltration of the malignancy[5–7]. Even without initial presentation of these symptoms, patients all have to endure a rigorous treatment plan and may also have adverse effects from toxicity associated with chemotherapy and/or an allogeneic hematopoietic stem cell

transplant (allo-HSCT). The implemented therapy may increase the risk of developing conditions such as cytopenia or neutropenia, due to its immunosuppressive nature.

1.1.2 Prognosis of patients

In general, children and adolescents with leukemia have a much better prognosis. In fact, despite ALL being the most common form of cancer in children aged 0-14 years, the observed five-year survival rate for children with lymphoid leukemia is 91%[3]. Those diagnosed at older ages, however, are not as fortunate. Five-year survival rates for adults under 60 years old is only 30-40%, and continues to decline rapidly for patients above 60[8]. This difference in survival is believed to be due to the positive therapeutic responses following aggressive treatment strategies, which are associated with significant toxicities that typically result in medical co-morbidities and longer lasting complications in older patients. Furthermore, leukemia in older patients is more likely to involve complicated genetic abnormalities. Risk stratification is an important component of diagnosis and prognosis as it informs the therapeutic strategy, and is based on a number of factors including age, white blood cell count at presentation and specific genetic mutations and translocations. Arguably the strongest predictive factor is response to induction treatment, which can now be monitored by assessing minimal residual disease (MRD)[8].

Some common translocations associated with ALL are t(12;21), t(1;19), and t(9;22), known as the Philadelphia chromosome and generating the fusion protein [*BCR-ABL1*][5]. It is important to note that other downstream genetic and epigenetic changes also occur leading to an aggressive disease course of ALL. Of the identified translocations, the Philadelphia chromosome translocation (Ph) has the greatest impact

on prognosis, as its presence indicates a very aggressive form of leukemia, with a high-risk of disease recurrence. It presents in approximately 20-30% of adult patients with ALL, and only about 10% of patients survive when receiving chemotherapy alone[9,10]. However, Ph-negative leukemia does not automatically indicate a low-risk prognosis. Other identified genetic markers have also been associated with poor outcomes such as low-hypodiploid ALL, t(4;11), t(8;14), as well as a Ph-like ALL, which closely resembles the genetic expression profile of Ph-positive ALL, but lacking the chromosomal rearrangement[5]. These genetic aberrations can be crucial towards determining a treatment strategy as they can predict response and outcome. Diagnostic parameters such as white blood cell count and genetic expression of ALL dictate the initial therapy given to patients and their prognosis. However, patients' response to induction therapy, by monitoring MRD for example, is crucial in determining an updated prognosis and further treatment. The risk stratification process demonstrates the heterogeneity associated with ALL and is important to consider when developing new therapeutic strategies.

1.1.3 Standards of care

For patients with ALL, the first line of induction therapy usually consists of aggressive multi-agent combination chemotherapy, under which many patients achieve their first state of complete remission (CR1). After induction chemotherapy, all patients in CR1 will go on to receive consolidation/maintenance chemotherapy treatment, unless they are eligible to receive an allo-HSCT and have an available donor for this procedure. Typically, this procedure is not recommended in CR1 unless the patient is considered to be high-risk and likely to relapse based on the risk stratification

parameters discussed above. The prominent reason to not expose all patients to HSCT is the associated morbidity and mortality with this procedure. Graft versus host disease and graft failures are common effects after receiving a transplant, and this can greatly reduce quality of life or even lead to mortality[11]. Improving survival rates after transplant is also desired, because the therapy itself is not always effective at reducing relapse rates or achieving CR status. One study found a 10 year overall survival rate of only 35%, therefore urging for the advancement and improvement of curative therapies[11]. Some advances have been made in regards to induction therapy recently, by way of tyrosine kinase inhibitors (TKI), which target the protein rearrangement formed in Ph+ ALL. Imatinib, a first generation BCR-ABL-targeting TKI was introduced as a single-agent therapy for chronic myelogenous leukemia (CML) since the Ph chromosome translocation is present in over 90% of CML cases[12]. From a study of 553 CML patients treated with imatinib, an 85% overall survival rate was found 8 years after diagnosis[13]. As a single agent therapy for relapsed or refractory Ph+ ALL, imatinib generated response rates of 30%, but these were not sustainable as median overall survival was just under 5 months[14]. In combination with chemotherapy, imatinib improved CR rate in chemoresistant patients from 60% to 96%[15]. Overall survival at 18 month follow-up also improved from 39% to 65%, keeping in mind that 56% of CR patients under 40 years old received a stem cell transplant[15]. Since then, 2nd and 3rd generation TKIs have increased the number of Ph+ ALL patients eligible for transplant due to decreasing early death rates and disease recurrence as well as increasing rates of CR[16]. While these compounds may improve response rates after induction therapy,

they are not sufficient to overcome the need for stem cell transplantation for the best chance at long-term survival[17,18].

Recent advances in clinical trials have led to exciting new immunotherapeutic strategies with better potential for long-term cures and survival. For instance, there have been a number of clinical trials in the United States testing both the efficacies of bispecific T cell engagers (BiTE) and chimeric antigen receptor (CAR) T cells. These promising therapies have mainly been investigated for patients with relapsed or refractory ALL who have otherwise limited options. Both of these immunotherapies have thus far taken advantage of using CD19 as a target antigen for B-cell ALL because it is a marker commonly found in this disease[19–21]. One BiTE called blinatumomab, is an antibody construct that allows CD3 expressing T cells to identify and kill CD19 expressing lymphoblasts. When tested against standard chemotherapy for B-cell precursor ALL, it increased the overall survival time for patients by 3.7 months and increased the rate of event-free survival at 6-month estimates from 12% to 31%[21].

These immunotherapies have shown promising results so far and are currently the best treatment options for patients with aggressive ALL. However, while both CAR T cell and BiTE therapy provide a survival advantage over standard chemotherapy, the majority of patients still relapse. Roughly 80% of B-ALL patients treated with blinatumomab showed clearance of MRD, but a second study found only 43% of relapsed/refractory B-ALL patients achieved CR[22,23]. Further follow up of this study revealed that in the absence of subsequent allo-HSCT, 67% of patients relapsed[24]. Similarly, a pediatric study investigating CD19 CAR T cell therapy found 93% of patients in CR after 1 month, but only 55% were disease-free 1 year after treatment[25].

There is still much work to be done in order to better understand the mechanisms of resistance to these therapies such as CD19 negative relapse, as well as their adverse effects, including cytokine release syndrome[26,27]. Only those with B-lineage tumour cells expressing CD19 can benefit from these targeted therapies, which, fortunately represents over 98% of B-ALL patients[28]. While these examples underscore the immense potential benefit of immunotherapy in the treatment of refractory or relapsed B-ALL, therapies capable of inducing long term survival while minimizing recurrence and therapy-induced toxicities are still needed.

1.2 Cancer therapeutics

1.2.1 Oncolytic viruses

Another particularly interesting field within biotherapeutics is that of oncolytic virotherapy (OV). Certain lytic viruses are able to infect cancerous cells, and several have been well characterized for their oncolytic potential. Many viruses under current investigation have been genetically altered to enhance their efficacy and selectivity, naming them 'oncolytic'. For instance, vesicular stomatitis virus (VSV) containing a deletion of methionine in position 51 of the matrix protein (VSVΔ51), showed decreased tropism for healthy cells, but retained its oncolytic capabilities[29]. Similarly, a double mutated Maraba virus (MG1) was found to be more selective and effective than its wildtype counterpart[31]. The increased selectivity is partly based on commonly found differential expression of certain genes in cancer cells, including interferon-stimulated genes (ISGs). The ability to genetically alter viruses, either by inducing mutations like those described above, deleting genes such as thymidine kinase in Vaccinia or encoding transgenes be they cytokines such as GM-CSF, or reporter genes like GFP and β-

galactosidase are attractive features of OVs and contribute to the ever-growing library of viruses under pre-clinical investigation[30,33,34]. DNA viruses, such as Herpes simplex, adenovirus and Vaccinia, as well as RNA-based viruses including Measles and rhabdoviruses, like VSV and Maraba, are all currently being investigated in clinical trials for therapeutic efficacy as OVs[29–33].

Therapeutic efficacy of OV infection is achieved by two major arms: direct oncolytic activity through lysis of tumour cells, as well as virus-induced secondary effects such as the induction of a systemic immune response. This can, in turn, prompt not only an antiviral response, but also a simultaneous anti-tumour response. This revelation has led to an ongoing interest in arming OVs with stimulatory cytokines to enhance and propagate stronger anti-tumour responses. Currently, OVs are also being investigated in combination with immune checkpoint inhibitors, in the hopes of enhancing the anti-tumour immune response further[35,36]. In 2015, the first OV (talimogene laherparepvec) was approved by the US Food and Drug Administration for treatment of metastatic melanoma[30]. While early trials have been promising, there is still room for improvement, and current work revolves around optimizing and enhancing OV efficacy to broaden their impact and prove it to be an accessible therapy.

1.2.2 Maraba MG1 rhabdovirus

The Maraba rhabdovirus has been employed during research in the lab partly due to its ease of replication, high titer propagation, and genetic cloning capabilities. Although in the same family, other common rhabdoviruses, including rabies and VSV, possess differences regarding their replication cycles, host tropism and virus-induced pathology[31]. Maraba was found to be an oncolytic candidate based on its rapid virus

production as well as its cytolytic activity against many cancer cell lines[31]. As it is a vesiculovirus, it shares genomic structure with VSV consisting of 5 genes: matrix (M), nucleoprotein (N), phosphoprotein (P), glycoprotein (G) and RNA-dependent RNA polymerase (L). The commonalities with VSV lead to the same potential for specific mutations to generate an attenuated virus, as was the case for VSVΔ51. Based on these previous findings, Maraba MG1 containing mutations in both the M and G proteins (L123W and Q242R, respectively) was attenuated in primary normal human fibroblast cells, but in fact was more cytolytic to tumour cells than wildtype Maraba virus[31].

Rhabdoviruses are known to mediate host cell entry by receptor-mediated endocytosis[37]. Beginning with receptor binding, the virus envelope glycoprotein interacts with host cell-surface receptors. In the case of MG1 and VSV, the host transmembrane LDL receptor protein serves as a major binding protein, although other members of this protein family can also function as receptors[38,39]. There is evidence that rabies virus binds to both the nicotinic acetylcholine receptor and the neural cell adhesion molecule[40]. Since VSV has been studied in great detail, the following steps have been detailed for this particular rhabdovirus. Following receptor binding, the virus enters either newly formed or pre-generated clathrin-coated pits within the plasma membrane[41,42]. From here, the virus enters the host cell via the endosome pathway. The release of the virus into the cytosol is a two-step event, although a more direct one-step pathway has also been identified. Fusion is facilitated by the viral glycoprotein, which is reversibly dependent on the compartment acidity and occurs with the internal vesicles in sorting endosomes, also known as multivesicular bodies.[37,41] These VSV-containing internal vesicles then undergo 'back-fusion' with the

limiting endosomal membrane for release of the nucleocapsid into the cytoplasm[37,40]. However, the back-fusion mechanism may not be required and in the absence of internal vesicle formation within multivesicular bodies, VSV was able to directly fuse with the early endosomal membrane[37,40]. With the cooperation of its few proteins including the viral RNA-dependent RNA polymerase, VSV transcribes its negative sense, single stranded RNA genome resulting in a positive sense RNA. Viral proteins are translated from this point, as well as additional transcription of the viral genome from the positive strand, allowing for negative-sense RNA genome replication[43]. Viral genome and proteins then assemble at the plasma membrane before exiting the cell.

Maraba MG1 virus has been optimized for attenuation in healthy cells and selectively engineered for its ability to lyse cancer cells. It also holds many advantages and mechanisms for improvement, such as its ability to incorporate transgene expression. All these aspects improve its outlook in clinical settings. It has also been used previously in the context of L1210 ALL studies, showing efficacy both *in vitro* and in an infected tumour cell vaccine model. Within this thesis, Maraba MG1 oncolytic virus was used for these reasons, with the hope to expand any results to a number of models and viruses alike, in the future.

1.2.3 Antibody-based therapeutics

Oncolytic viruses are not the only biotherapy aimed at generating a robust anti-tumour response. Antibody therapy is a targeted approach that has been shown to induce a response and survival benefit for some cancers. However, often and especially in the case of leukemia, cancers harbour antigenic variation, which can lead to selection of clonal populations lacking the antibody target and leading to therapeutic

resistance[44,45]. BiTEs, as mentioned earlier, augment the targeting of tumour cells expressing a specific antigen by guiding effector T cells to the antigen of choice and have shown considerable efficacy in patients[21]. However, within the same tumour, different cancer cells can show varying expression of a wide array of antigens, of which only some may be considered tumour-specific or even tumour-associated. In addition, therapy-resistant tumour cells have been identified in patients receiving CD19-targeted approaches, where CD19 expression is lost in order to maintain tumour survival and proliferation[26]. Therefore, an antigen agnostic therapy, one that can target a family of tumour-associated antigens simultaneously may provide a stronger and broader response. For these reasons, immunotherapies that have the potential to activate a response against many tumour-associated antigens provide an ideal course of action. Examples of this strategy are immune checkpoint inhibitors, which have shown survival benefits in a number of studies, and are also being researched in combination with OVs[46–48]. Here, an antibody targeting an inhibitory signaling receptor on an immune effector T cell, such as cytotoxic T lymphocyte antigen 4 (CTLA-4) or programmed cell death 1 (PD-1) receptor, is introduced to the body where it works to block the inhibition of this effector cell population against tumour antigens. This strategy draws on the fact that tumour microenvironments can be very immunosuppressive and while many innate and adaptive immune cells may be infiltrating the tumour, few are being fully activated and armed to attack tumour cells. The suppressive actions of tumour cell evasion such as downregulating major histocompatibility complex (MHC) expression, increasing suppressive cytokine expression, or binding to inhibitory signaling receptors like PD-1, along with immune

regulatory cell recruitment, like T regulatory cells or myeloid-derived suppressor cells, lead to inhibition of effector cells[49]. Checkpoint inhibitor therapy aims to reverse this environment by antagonistically blocking inhibitory signals on effector cells and promoting their activation and action.

1.2.4 Tumour cell vaccines

Whole tumour cell vaccines have also been investigated as anti-cancer therapies and have been shown to induce antitumour immune responses in some cases. Autologous or allogeneic tumour cells are first irradiated to arrest any cell growth or division, and then injected to stimulate an immune response against tumour antigens. A distinct advantage of whole cell vaccines is that the entire repertoire of antigens found throughout the tumour can be presented to the immune system under immune stimulating conditions. For instance, OncoVAX, a vaccine preparation incorporating autologous whole cells and bacillus calmette–guerin (BCG) has shown improved overall survival and reduced the risk of disease progression compared to control stage II patients with colon cancer[50]. In a model of murine colon carcinoma, an irradiated tumour cell vaccine did not improve outcomes unless combined with stem cell transplantation[51]. Additionally, an autologous cell vaccine using Newcastle disease virus (ATV-NDV), showed improved 5 year survival rates in patients with head and neck squamous cell carcinoma by 23% compared to standard therapy[52]. More often than not, it appears that the most effective whole cell vaccine strategies may include other adjuvants or treatments in combination, such as HSCT, cytokine expression or virus infection for additional immune stimulation and a greater antitumour response[53].

In fact, tumour cell vaccines incorporating OVs have since been researched in a number of cancer models. Here, tumour cells are irradiated as well as infected with an OV, before being injected as an infected cell vaccine (ICV). There are still many theories under investigation alluding to the exact mechanism of action, however it is generally believed that the presence of an OV enhances the immunogenicity of the tumour cells, and may contribute to the generation of an anti-tumour immune response. In leukemia, an ICV has been studied in a DBA/2 mouse model using the L1210 murine leukemic cell line[54]. From a number of experiments, it was determined that vaccinated mice can be fully and specifically protected from leukemic challenge, however its efficacy decreases with increasing tumour burden[54]. This is still remarkably impressive given that an irradiated whole tumour cell vaccine, or intravenous OV treatment alone, provides no survival benefit to mice with leukemic burden. It was also found that the virus infection and incubation time was critical to the efficacy of the ICV, such that a 1 hour infection instead of 18-20 hours, or separation of the virus and irradiated tumour cells caused treatment efficacy to suffer[54]. When comparing models of ICV, there can be stark differences, which mechanistically have not yet been explained. For instance, a solid tumour model of murine B16-F10 melanoma in C57BL/6 mice, showed some protection from ICV administration even with 2 hours of virus incubation time, perhaps due to the replicative capacity within the host cell[55]. Regardless of the model being studied, the ICV typically shows a greater therapeutic benefit than a whole tumour cell vaccine alone. This data points to OV infection being critical, and suggests that virus infection can enhance anti-tumour immune responses when introduced via ICV platforms. Therefore, cancer cells and tumour models that can be infected by OVs, are

much more likely to profit from the added benefits of an ICV as opposed to a tumour cell vaccine alone through the generation of a more robust anti-tumour immune response (Fig. 1). Enhancing virus infection and susceptibility in resistant tumour models would not only enhance viral oncolysis, but could also produce added benefits of rendering an ICV possible and stimulating an antigenically broad anti-tumour response. This type of therapy also creates many possibilities in the field of personalized medicine, and may provide patients who have chemo-resistant and/or non-resectable tumours with a targeted and practical therapeutic strategy. The limitations of up-and-coming immunotherapies discussed earlier, such as BiTEs and CAR T cells, are several and include the emergence of therapy-resistant clonal outgrowth and tumour relapse, cytokine release syndrome and the persistent requirement of allo-HSCTs. It is hoped that a personalized ICV could alleviate these drawbacks while improving long-term survival and quality of life.

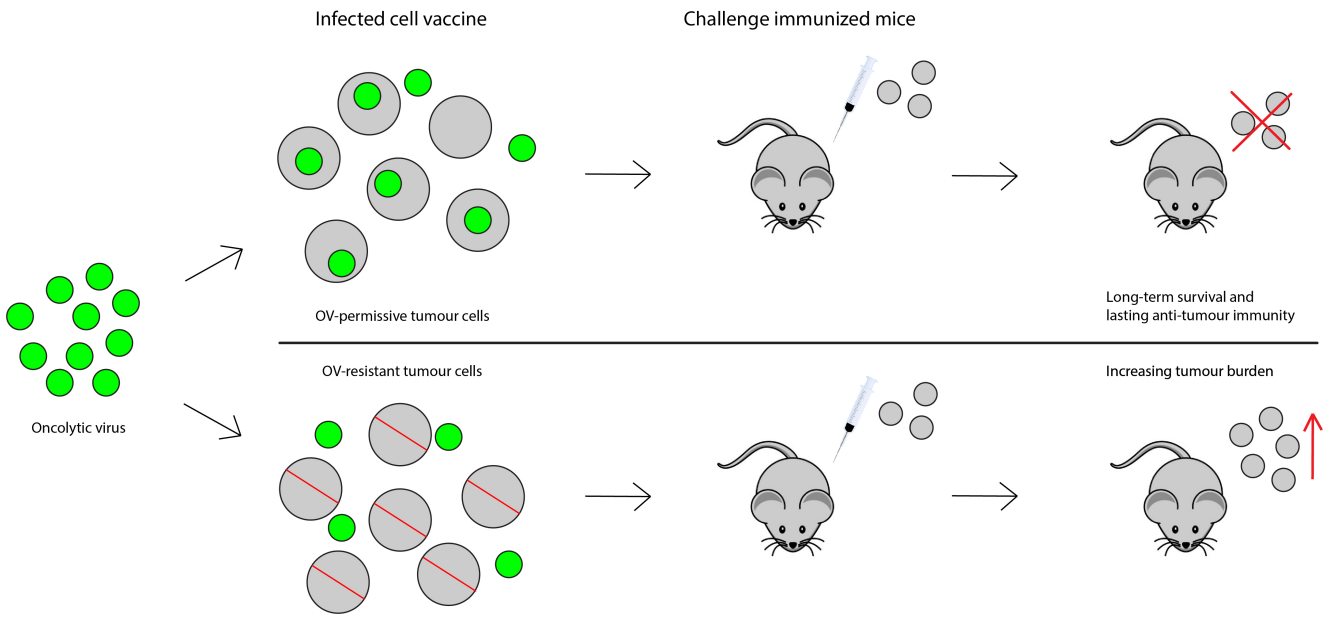
Infected cell vaccine
Challenge immunized mice
OV-permissive tumour cells
Long-term survival and
lasting anti-tumour immunity
OV-resistant tumour cells
Increasing tumour burden
Oncolytic virus

Figure 1. Predicted model of OV resistance on ICV efficacy. Since a complete lack of viral infection abrogates the efficacy of an ICV in a leukemia DBA/2 mouse model, it is predicted that a highly resistant cancer model would behave very similarly. Vaccines prepared with extremely resistant cancer cells would not be effective at producing the same protective, robust, lasting, anti-tumour immune response compared to susceptible tumour cells based on the impact OVs appear to have on tumour cell immunogenicity.

1.2.5 Mechanisms of resistance to virotherapy

While there are many mechanisms contributing to cancer cell resistance to viral infection such as pathways involved in virus entry, cell stress, apoptosis and virus release, the most notably studied is the antiviral impact of the interferon (IFN) pathway. In addition to their ability to modulate immune responses, IFNs also aid in regulating other processes like cell growth and differentiation. As mentioned, several genetically engineered viruses have been altered for increased attenuation upon type I IFN exposure; drawing on the general overall loss of type I IFN response in cancer cells[29,31]. Type I IFNs, including IFN-α and IFN-β, are cytokines ubiquitously recognized by almost every cell type. They provide signals important for protection against viruses and other intracellular infections. Cytokine production is instigated through recognition of viral nucleic acid binding to either soluble, cytosolic receptors such as RIG-I or MDA-5 proteins, or toll-like receptors (TLR) situated on endosomal membranes of specialized cells[56]. Ultimately, a combination of activated and translocated interferon regulatory factors (IRF) 3 and 7, as well as the nuclear factor kappa-light-chain-enhancer of activated B cells (NF-κB) transcription factor can enhance expression of type I IFN[57]. In the canonical pathway, type I IFN proteins can act in a paracrine and autocrine fashion through the type I IFN receptor in order to trigger expression of IFN-stimulated genes (ISG) through the Janus kinase (JAK)-signal transducer and activator of transcription (STAT) signaling pathway[56,58], leading to a broad antiviral state in which all stages of the viral life cycle may be inhibited. For example, RNA-dependent protein kinase (PKR) is an ISG, which inhibits translation by

phosphorylating eukaryotic translation initiation factor 2 (eIF2A) in the presence of double stranded RNA, a product which many viruses express during their replication[58].

Importantly, cells lacking type I IFN expression or response may still not be fully susceptible to virus infection as multiple steps are necessary for a productive infection (generation of viral progeny) to occur. For example, rhabdoviruses such as VSVΔ51 and MG1 first bind to the transmembrane low density lipoprotein (LDL) receptor[38,39]. LDL-receptor (LDL-R) is a transmembrane protein that otherwise functions to maintain plasma cholesterol homeostasis by internalizing extracellular ligands for degradation in lysosomes through receptor-mediated endocytosis[59]. Other members of the LDL-R family can also serve as viral binding proteins. This facilitates fusion and viral entry by clathrin-mediated endocytosis[60]. Cancer cells that lack *all* expression of this membranous protein family, will be resistant to rhabdovirus infection by VSVΔ51 or MG1[38,39,61].

Viral biology is still a hot research topic, especially as far as OVs are concerned. While many pieces of the puzzle have been filled in and discovered over the years, there is most likely much more information to uncover regarding the biology of a viral infection as well as cell biology as it pertains to viral resistance. Understanding the various mechanisms and pathways that may be involved in rendering a cell susceptible or resistant to an OV would make a large impact on how researchers approach optimizing this therapeutic strategy as well as how OV-based immunotherapies, like an ICV, are designed and used in a clinical setting.

1.3 CRISPR technology

1.3.1 Generation of loss-of-function mutations

Clustered regularly interspaced short palindromic repeats (CRISPR) and the CRISPR-associated protein 9 (Cas9) enzyme are the hallmarks of the CRISPR-Cas9 system. Within the bacterial origin of this system, these repeats are separated by 'spacers' in the DNA, which are derived from bacteriophage genomic material in order to prevent future infection[62,63]. Alongside the bacterial Cas enzyme, the bacteria incorporate these small segmental pieces of the viral genome in order to recognize and direct the targeting of double strand breaks to the same sequences in the future, acting like a bacterial 'immune system'[63,64]. The Cas9 enzyme isolated from *Streptococcus pyogenes,* has since been adapted for use in various applications, including modifying and editing genomic DNA in cell lines and organisms alike[65–67]. In the lab, the bacteriophage spacer sequences are replaced with a single 20-nucleotide guide RNA (gRNA) molecule[64]. The gRNA and Cas9 enzyme can be introduced together, or separately, via various methods including transient transfection, electroporation or lentivirus transduction[68,69]. The Cas9 enzyme uses this gRNA to direct genomic cleavage, resulting in the production of a double strand break (DSB) at the DNA site complementary to the gRNA sequence within the host genome. Since Cas9 enzyme uses recognition of not only the complementary region, but also a protospacer adjacent motif (PAM) sequence (NGG), gRNAs are designed to bind directly upstream from one of these sequences[64]. After recognizing this break, the cell initiates its genomic repair mechanisms, namely one of either homologous recombination (HR) or non-homologous end joining (NHEJ)[70]. If no DNA template is present, NHEJ, which is typically very error-

prone is used as the dominant repair mechanism[70]. In the case of generating a knockout or loss of function mutation in a gene, NHEJ is desired due to small insertions or deletions causing a frameshift in the genomic sequence[71]. Each gRNA has a unique cleavage efficiency based on its binding site, but the CRISPR-Cas9 system has now been used extensively worldwide and shows high efficiency for creating gene knockouts at most loci.

1.3.2 Genome-wide screens

Genome-wide approaches offer a powerful and unbiased method for identifying unanticipated regulators of biological phenomena such as viral infectivity. Due to its ease of use, ability to edit virtually all sequences in the genome and limited off target effect, CRISPR-Cas9 has rapidly become a preferred tool for genome wide screening. Numerous gRNA libraries targeting the entire human or murine genome can be purchased commercially in the form of DNA plasmids[69,72]. The libraries have been designed so that each gene is targeted multiple times in different regions to maximize mutation rate and ensure that each gene is in fact targeted. For example, the murine genome wide CRISPR knockout (mGeCKO) version 2 library contains 130,209 gRNAs against 20,611 genes, where each gene is targeted by 6 gRNAs[69]. The library also contains non-targeting control sequences which are used as transduction and selection controls. There are two common methods of introducing the library as well as the Cas9 enzyme into the cell line of choice. In a two-step system, cells can first be transduced and selected to express Cas9 protein, followed by the addition of the gRNA lentiviral library transduction. Alternatively, cells can be transduced with lentiviral constructs that contain both the Cas9 enzyme and a unique gRNA sequence. Following

transduction, antibiotic selection is used to ensure the survival of only those cells in which the lentivirus was successfully integrated. Following selection of the cell library, a researcher may explore seemingly endless possibilities, including identifying mechanisms of drug resistance and treatment susceptibility to name a few.

1.3.3 Identifying treatment resistant cell populations

The GeCKO CRISPR screens have been applied to a number of different contexts and have proven extremely useful in identifying genes and pathways as they relate to various outcomes. Some of the first published data using this genome-wide format involved the identification of genes essential for cell survival or proliferation[72]. The libraries have also been used to identify means of drug resistance, indicating that both negative and positive selection can be achieved[72,73]. They have been employed to determine genes required for cell-cell interactions and the effector functions of T cells within the immune regulatory network[74]. In addition to the numerous *in vitro* studies, there have also been several groups using CRISPR screens *in vivo*. For instance, primary cells derived from a Cas9 transgenic mouse were used for one study that was interested in genes that control the induction of tumour necrosis factor in the host response to pathogens[75]. Conversely, *in vivo* metastasis was an outcome for a study that performed a genome-wide screen in a non-metastatic mouse cancer cell line, where gene knockouts that induced metastasis were identified[66].

Genes and mechanisms of drug resistance have already been identified with the GeCKO screen format *in vitro*, and considering how often treatment resistance arises, more investigative studies like this may provide very useful, especially in cancer research. Along the same line, a genome-wide library screen could also extend a hand in

determining mechanisms of OV resistance. Therapies drawing largely on the effect of OVs could be extended to more models of disease if viral resistance was better understood. Perhaps then, resistant cancers could be made more susceptible to OV infection, leading to higher direct oncolysis as well as a better chance of utilizing emerging OV-based immunotherapies like ICV.

1.4 Hypothesis

A genome-wide CRISPR screen in a susceptible acute lymphoblastic leukemia cell line, L1210, will identify novel genes that contribute to the susceptibility of tumor cells to oncolytic viruses.

1.5 Research objectives

1. Perform a genome-wide CRISPR screen in the L1210 cell line and identify gene knockouts that render the cell line resistant to MG1 infection.
2. Generate an L1210 cell line carrying a gene knockout for the LDL receptor and validate its effects on Maraba MG1 infection as well as the L1210 DBA/2 ICV model.
3. Compare two tumour models of L1210 leukemia in DBA/2 mice to identify any variation in the protective effects of an ICV.

Chapter 2: Materials and methods

2.1 Reagents

Blasticidin antibiotic was supplied by InvivoGen and puromycin selection antibiotic by Cayman Chemicals. All DNA primers were ordered from Integrated DNA Technologies. Universal type I IFN-α (catalog #11200) was obtained from PBL Assay Science. Flow cytometry stain, ethidium homodimer-1 (catalog #E1169), was obtained from ThermoFisher. Immunoblots were stained with the following antibodies: CRISPR/Cas9 monoclonal antibody (catalog #C15200203) from Diagenode, murine LDL receptor antibody (catalog #AF2255-LD) from R&D Systems, GAPDH monoclonal antibody (catalog #2118s) from New England Biolabs (NEB), and secondary antibodies goat anti-mouse (catalog #115-035-003), goat anti-rabbit (catalog #111-035-003) and bovine anti-goat (catalog #805-035-180) from Jackson Immunoresearch. Recombinant murine LDL receptor was a kind gift from the Diallo lab. The lentiviral packaging plasmids pMD2.G (catalog #12259) and psPAX2 (catalog #12260) as well as the lentiGuide-Puro vector (catalog #52963) were purchased from Addgene. The 2-vector system murine genome-wide CRISPR knockout (mGeCKO) library version 2 as well as the lentiCas9-Blast plasmid was also obtained from Addgene (catalog #1000000053).

2.2 Cell lines

American Type Culture Collection (ATCC) supplied all cell lines: murine B cell acute lymphoblastic leukemia L1210, monkey epithelial Vero, and human embryonic kidney HEK293T. Cells were cultured at 37°C and 5% CO_2, in Dulbecco's Modified Eagle Medium (DMEM) with 10% fetal bovine serum (FBS) except Vero cell media contained 10% of a 3:1 ratio of newborn calf serum (NCS):FBS.

2.3 Viruses

Oncolytic virus Maraba MG1 expressing GFP (MG1-GFP) was propagated by infecting Vero cells at a multiplicity of infection (MOI) of 0.01 until approximately 50% of cells had detached (24-48 hours), at which point, media was collected and centrifuged at 1500xg for 5 minutes at room temperature to pellet and remove cell debris. Supernatant was then run through a 0.22μm filter before centrifuging the viral pellet at 14,000rpm and 4°C for 90 minutes. Supernatant was aspirated and the virus was resuspended in phosphate-buffered saline (PBS) before storing aliquots at -80°C.

Virus stock concentrations were determined through plaque assays, where Vero cells were seeded in triplicate and infected with serial dilutions of virus stock in serum-free media. This was replaced after 1 hour of incubation with an overlay media of 50% 6% carboxymethyl cellulose, 40% DMEM and 10% FBS. Cells were cultured for an additional 48-72 hours, until plaques became visible. Lastly, cells were washed with PBS, stained with 1% crystal violet and let dry in order to count plaques present. Concentration was determined with the following equation:

$$Titer\left(\frac{pfu}{mL}\right) = \frac{\#\ of\ plaques\ per\ well}{(dilution\ of\ viral\ stock)(volume\ of\ virus\ stock)}$$

2.4 Mice

DBA/2 mice were purchased from Charles River laboratories at 6 weeks of age and housed in biosafety level 2 facilities at the University of Ottawa under Canadian Counsel of Animal Care guidelines. All experiments were conducted according to institutional Animal Care and Veterinary Services requirements. Endpoint of mice bearing subcutaneous L1210 tumours was determined by a tumour size greater than 225mm^3 (15x15mm) and systemic leukemia bearing mice reached endpoint when

leukemia developed with any symptoms of respiratory distress, hind limb paralysis and/or solid tumour masses.

2.5 ICV preparation and administration

L1210 cells at 1e6 cells/mL were first infected at MOI 10 with MG1-GFP and cultured for 18-20 hours. Cells were then washed twice in PBS after counting viable cells by trypan blue exclusion with ViCell counter (Beckman Coulter). The culture was resuspended in PBS at a final concentration of 1e7 viable cells/mL. Infected cells were finally γ-irradiated with 30 Gray (HF320, Pantak). The vaccine was administered via the tail vein of mice at 1e6 cells per animal. All experiments consisted of 3 ICV doses, each given in weekly intervals, unless otherwise stated.

2.6 Leukemic challenge

The intravenous (IV) leukemic challenge of viable L1210 cells resuspended in PBS was injected via tail vein at 1e6 cells per animal, 7 days after the last ICV. Some experiments consisted of a subcutaneous (SQ) leukemic challenge of viable L1210 cells injected under the skin of the right flank, while mice were anesthetized with isoflurane, also 7 days after the final ICV dose was administered.

2.7 Antibiotic selection curve

Puromycin and blasticidin antibiotics were tested on L1210 cells to determine the threshold concentration for treatment-induced cytotoxicity. L1210 cells were seeded in suspension culture and antibiotic was added at varying concentrations ranging from 1-5μg/mL. After 5 days, cells were analyzed by flow cytometry for viability compared to untreated samples (section 2.16).

2.8 Lentivirus DNA transfection

Successfully cloned lentivirus DNA was transfected into the media of HEK293T cells, along with envelope plasmid pMD2.G containing VSV-glycoprotein and packaging plasmid psPAX2 (Addgene). TransIT-LT1 transfection reagent (Mirus) in Opti-MEM media (Gibco) was added simultaneously and incubated for 8 hours before replacing with normal media. Lentivirus-containing supernatant was harvested 24, 48 and 72 hours post transfection. Supernatant collections were pooled and filtered using a 0.22μm threshold and stored in aliquots at -80°C.

2.9 Lentivirus transduction

Cells were seeded to 50% confluency before adding lentivirus to the media. Lentivirus was incubated on cells for 24 hours until the media was replaced and puromycin or blasticidin was added at a concentration determined by an antibiotic kill curve. For all L1210 cell experiments, antibiotic at 4μg/mL was incubated on cells for at least 5 days.

2.10 Cas9 stable expression and characterization

LentiCas9-Blast plasmid DNA (Addgene) was amplified and transfected to generate infectious lentivirus particles as per section 2.8. Infectious lentivirus was transduced into L1210 cells as per section 2.9. Single cell clones were sorted and isolated by flow cytometry (section 2.16) and incubated in culture to expand. Cell lysates were collected and analyzed by immunoblot for Cas9 expression and GAPDH expression as a control (section 2.17). Cells were also seeded in culture along with control (untransduced), wildtype L1210 cells for 7 days. Cell suspension was analyzed for cell growth characteristics by resazurin assay (section 2.19) 1, 2, 3, 6 and 7 days

after seeding. Functionality of the expressed Cas9 enzyme was assessed in each clonal cell line by transducing biological replicates of cells with lentiviruses containing gRNAs targeting essential genes (*Psmd1* and *Psmb2*) according to section 2.9. Functional Cas9 enzyme would effectively target the essential gene upon expression of gRNA, and the cells would no longer be viable, as a result. As a control, a sub-culture of cells was transduced with pLKO.1 control lentivirus that does not contain any genomic Cas9 or gRNA sequences. Resazurin assay (section 2.19) was performed 10 days following puromycin selection at 4μg/mL to assess cellular viability through metabolic activity. Lastly, clonal Cas9-C cell line replicates were either mock-infected or infected with MG1-GFP virus at an MOI of 1 by adding virus directly into cell culture and incubating over the course of the experiment. Resazurin assays determined cell metabolic activity (and viability) 24 and 48 hours after infection.

2.11 Type I IFN pre-treatment and infection

Wildtype and Cas9-expressing L1210 cells were seeded for triplicates per experimental condition. Each condition consisted of either mock-infection, treatment with universal type I IFN at 50U/ml for 4.5h, infection with MG1-GFP at an MOI of 0.1, or treatment with IFN at 50U/mL for 4.5h followed by infection with MG1-GFP at MOI 0.1. Virus was incubated in cell culture for the total time of the experiment. A resazurin assay (section 2.19) was performed 18 and 42 hours post infection.

2.12 CRISPR genome-wide screen

The murine GeCKO library version 2 (Addgene) plasmid DNA was first electroporated and amplified in DH5-α bacteria (NEB). A total of 400ng of each library half was electroporated at 1.5kV, 25μF and 200Ω. Transformed bacteria was spread

onto plates and grown overnight at 32°C. Bacteria was then scraped off with LB media and centrifuged before isolating by maxi prep (Qiagen). Purified plasmid DNA was then transfected as described earlier (section 2.8) in order to produce infectious lentiviruses. Supernatant was collected 48 hours post transfection.

The concentration of the lentiviral stock was determined by transducing a set number of cells with varying volumes of lentivirus preparation. Cells were selected with media containing 4μg/mL of puromycin for 5 days, and analyzed for viability by flow cytometry. The percentage of viable cells following transduction represented the percent of lentivirus-integrated cells, as well as the concentration of lentiviruses in the stock volume used. This information and the antibiotic curve data was then used in determining how many cells to initially transduce in order to represent the library by 250 fold after puromycin selection and infect at an MOI of 0.3 for 30% infected cells, so to minimize the number of cells with multiple transductions[66,76] and so that each gRNA is present in at least 250 cells, with the following equation:

$$\#\ of\ cells\ to\ transduce = \frac{(\#gRNAs\ in\ library) * (\#\ cells\ per\ gRNA)}{\%\ viable\ cells\ after\ transduction\ \&\ selection}$$

One day following transduction of 130e6 cells with the lentivirus library, cells were selected in 4ug/mL of puromycin for 5 days, after which point 2e6 cells were analyzed for viability by flow cytometry. When selection was complete (T0), cells were split into triplicates of 35e6 cells to maintain gRNA representation and cultured for 12 days, splitting cells every 6 days.

Each triplicate was then split further: 35e6 cells of each to a mock population and 60e6 cells to each replicate of virus infection. Cells were infected with MG1-GFP at either an MOI of 0.1 or 10, each in triplicates of 60e6 cells. Media was replaced for

infected cells every 3-4 days and mock cells were split every 7 days to maintain gRNA representation. 72 hours post virus infection, 30e6 cells of two replicates (Replicate A, MOI 10 and Replicate B, MOI 0.1) were flow sorted for viability and lack of green fluorescence. Throughout the screen, viability was monitored by trypan blue exclusion. Every time mock cells were split, 35e6 cells from each triplicate were spun down and frozen at -20°C for future genomic DNA extraction. Infected cells were only collected and frozen for DNA extraction once viable cell number and percentage viability increased in order to maintain library representation in both collected and cultured samples.

Screen cell samples were re-infected 99 days after the primary MG1-GFP infection. Cells from each condition were cultured in triplicates of both mock-infected and MG1-GFP secondary-infected wells. MG1-GFP was added at an MOI of 1 and cultured for 40 hours, until metabolic activity and viability were assessed by resazurin assay (section 2.19)

2.13 Screen DNA extractions and PCR reactions

Frozen cells were thawed and genomic DNA was extracted according to DNeasy Blood and Tissue kit (Qiagen) and quantified using a NanoDrop ND-1000 (ThermoFisher). Samples were prepared by first running a number of polymerase chain reactions (PCR), to amplify the region within the genomic DNA where the common lentiGuide-Puro vector integrated, which was a consistent sequence in all transduced cells. This region also contained the gRNA for which each cell expressed after integration, which served as the sequence of interest to deduct which genes were mutated in analyzed samples. These first PCR amplifications consisted of 72 reactions

at 50µL-100µL, performed with Q5 Hot Start High-Fidelity 2x master mix (NEB) using 3µg DNA per reaction in order to cover 215µg DNA per sample (assuming 6.6pg genomic DNA per cell). The primers used are (5'-3'):

Forward: CCCGAGGGGACCCAGAGAG
Reverse: AAGGGCCATAACCCGTAAAG

Reactions were pooled and used as template for a second PCR reaction used to barcode samples. Primers were designed to include vector-annealing, stagger and 8 base pair barcode sequences. They also included one of the p5 and p7 sequencing primer regions, which were used to bind the flow cell during deep sequencing (Fig. 2). These segments are part of the TruSeq universal adapter and were consistently added to all samples amplified with PCR 2. Each individual sample was amplified using a unique combination of forward and reverse barcode sequences to allow for de-multiplexing following a pooled sequencing strategy. The barcode-containing primers are listed in the Appendix, Table 2. 10µL of pooled PCR1-amplified sample was used as a template for each 50uL reaction, and 13 reactions were performed per sample. Both PCR reactions followed the same protocol with the exception of different annealing temperatures: denaturation at 98°C for 30 seconds, 20 repeated cycles of 98°C for 10 seconds, 62°C (PCR 1) or 67.4°C (PCR 2) for 20 seconds, and 72°C for 90 seconds, followed by 72°C for an additional 2 minutes and a 4°C hold.

The second PCR reactions were pooled for each sample and column purified with the PureLink PCR Purification kit (Invitrogen). This product was then run on a 1% agarose gel for gel extraction using the QIAquick gel extraction kit (Qiagen).

PCR 1 product

PCR 2 product

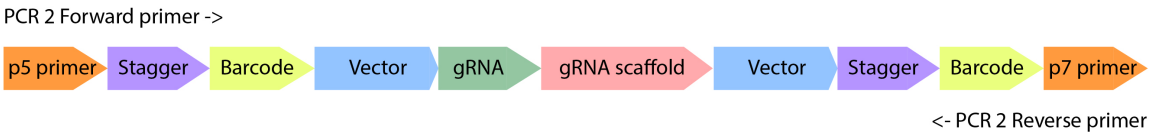

Figure 2. PCR amplified products of screen samples. A. PCR 1 amplified the region within the genomic DNA of all collected cell screen samples that included the lentiGuide-Puro backbone integration site, and therefore, the gRNA expressed. PCR 2, using PCR 1 product as a template, amplified a smaller overall sequence encompassing the gRNA expression site while incorporating unique stagger and barcode sequences to each direction as well as the p5 and p7 sequences required for deep sequencing and flow cell binding through the forward and reverse primers.

Finally, gel extracted samples were quantified by both NanoDrop and Quant-IT PicoGreen dsDNA assay kit (ThermoFisher), according to the manufacturer's protocol. Samples were deep sequenced by Fasteris (Switzerland) using Illumina HiSeq2500 and data were analyzed using Model-based analysis of genome-wide CRISPR-Cas9 knockout (MAGeCK) pipeline software.

2.14 MAGeCK test command

Read counts were analyzed prior to inputting into MAGeCK tests. Deep sequencing results were first normalized to reads per million (rpm). gRNAs absent from library plasmid samples and all subsequent samples were removed from the data. Each timepoint was further sorted to remove gRNAs whose expression was zero in at least 2 mock replicates. In the MAGeCK test command prompt, control labels were given to mock-treated replicates and treatment labels to infected triplicates at each timepoint. No normalization method was included due to prior analysis. The false discovery rate (FDR) was added as a gRNA-level p-value adjustment method and a positive sorting criteria was included.

2.15 Targeted gRNA cloning and validation

Cloning of individual gRNAs into the lentiGuide-Puro backbone (Addgene) for targeted CRISPR knockout experiments first involved identifying gRNA sequences from the murine GeCKO CRISPR library (Addgene). DNA oligos of both complements of the gRNA sequence with the appropriate 5' and 3' overhangs were ordered from IDT. The forward strand included a CACCG 5' overhang, whereas the reverse oligo contained a 5' addition of AAAC and C as a 3' overhang. The oligo sequences for LDL-R targeting were ordered as follows:

Forward: CACCGATCGGAGCCATCCGGGCACT
Reverse: AAACAGTGCCCGGATGGCTCCGATC

The oligos were annealed by combining both sequences at 100μM each with 10x T4 ligation buffer (NEB), T4 PNK (NEB) and distilled water at the following parameters: 37°C for 30 minutes and 95°C for 5 minutes before ramping down 5°C per minute until 25°C. The lentiGuide-Puro backbone was digested using 5ug of template, FastDigest Esp3I restriction enzyme (ThermoScientific), FastAP (ThermoScientific), 10x FastDigest buffer (ThermoScientific), 1mM DTT and distilled water at 37°C for 30 minutes. The following PCR ligated the annealed oligo gRNA sequence to the digested lentiviral backbone: 50ng digested plasmid, 1ul of annealed oligos, 1x Quick Ligase Buffer (NEB), Quick Ligase (NEB) and distilled water at room temperature for 10 minutes. Ligated DNA was then transformed into Stbl3 bacteria and harvested using Plasmid Plus Maxi kit (Qiagen). Lentivirus plasmid DNA was then transfected into HEK293T cells according to section 2.8 and lentiviruses were transduced to L1210-Cas9 expressing cells and selected with puromycin as per section 2.9. Clonal cell populations were isolated by single cell sorting flow cytometry (section 2.16) into individual wells of 96-well plates and expanded in culture. Clonal cell cultures were analyzed for LDL-R expression by collecting lysate and performing immunoblots (section 2.17) as well as for cell growth characteristics by comparing metabolic activity to wildtype L1210 cells expressing Cas9 through resazurin assay (section 2.19). DNA mutations were validated with Sanger sequencing with the following sequencing primers that annealed to the *Ldlr* murine gene sequence:

Forward: GTCACCTCTGTTGCGTTCTC
Reverse: GGTTGAGACTCACGGGAAGA

2.16 Flow cytometry staining and cell sorting

Viability staining was performed using ethidium homodimer-1 (EthD-1) at 0.1% v/v. Cells were counted, washed in PBS, and resuspended in flow buffer (PBS, 5% BSA) for 1-2e6 cells per sample. Stain was added immediately prior to running on the CyAN ADP9 flow cytometer (BD FACSCelesta, BD Biosciences). Single cell sorting was achieved with the MoFlo Astrios EQ cell sorter (Beckman Coulter), gating on viable cells from forward vs. side scatter plots, and sorting individual cells into separate wells of a 96-well plate. Pooled cell sorting after CRISPR screen infection (section 3.10) selected for cells gating on viability by EthD-1 staining and no GFP fluorescence.

2.17 Immunoblots

Cell lysates were collected by incubating cells on ice in RIPA lysis buffer for 10 minutes. This preparation was then centrifuged at 14,000rpm at 4°C for 15 minutes and supernatant was isolated and stored at -20°C. The concentration of protein in collected lysates was determined with the Pierce BCA Protein Assay Kit (ThermoFisher) as per the manufacturer's protocol. Each blot was loaded with 15ug of protein per sample onto a NuPAGE 4-12% Bis-Tris gel (Invitrogen). Gels were run at 200V for 60 minutes and wet transferred onto PVDF membranes at 100V for 90 minutes. Membranes were then blocked with 5% skim milk powder in tris-buffered saline, 0.1% tween-20 or TBS-T (20mM Tris, 150mM NaCl, pH 7.6, 0.1% Tween-20) for 30-60 minutes before adding primary antibody for overnight incubation. All antibodies were diluted in a solution of 5% bovine serum albumin (BSA) in TBS-T as follows:
Goat anti-LDL receptor: 1/500 (R&D Systems), Rabbit anti-GAPDH: 1/50000 (NEB), and HRP-conjugated secondary bovine anti-goat, goat anti-mouse and goat anti-rabbit

(Jackson Immunoresearch): 1/5000. Mouse anti-Cas9 (Diagenode) was diluted in 5% skim milk powder in TBS-T to a dilution of 1/1000.

Before adding secondary antibody for 60 minutes, membranes were washed 3 times with TBS-T for 10 minutes each. Finally, membranes were washed, reacted with SuperSignal West Pico PLUS Chemiluminescent substrate (ThermoFisher), and developed to visualize staining.

2.18 Giemsa staining of bone marrow and blood

Blood was collected from mice by cardiac puncture and bone marrow was isolated from femur and tibia bones. Blood was smeared directly onto slides and bone marrow dabs were done by firmly pressing exposed marrow onto slides. All slides were fixed with 100% methanol. When flushing bone marrow, bones were cut to expose marrow and placed in an Eppendorf tube containing a PCR tube with holes in the bottom. Tubes were then centrifuged for a short spin until the speed reached 16000xg. Pellets were resuspended in 500µL of PBS. A small aliquot (100µL) was centrifuged for 1 minute at 400xg and resuspended in sterile H_2O. This preparation was counted by trypan blue exclusion and 2e5 cells were added to a microscope slide and smeared slightly before letting dry and fixing with 100% methanol.

Giemsa-wright stain was a kind gift from the Stanford lab. The stock 1:1 solution was added directly onto each slide for 2 minutes. Slides were then incubated in a 1:20 solution (Giemsa stain in MilliQ H_2O) for 5 minutes. MilliQ H_2O was then used to thoroughly rinse slides before letting them dry.

2.19 Resazurin assay

Resazurin sodium salt was obtained from Sigma-Aldrich and resuspended in distilled water 0.05g/mL. Stock solution was further diluted to $1.3x10^{-4}$g/mL and stored at 4°C. This solution was added directly to wells of cell culture for evaluation of metabolic activity at 10% total well volume. Cells were then incubated at 37°C for 2-5 hours or until control, viable samples' media turned pink in culture. Samples were evaluated in 96-well plate formats on a Fluoroskan Ascent (ThermoScientific) by reading excitation at 530nm and emission at 590nm.

Chapter 3: Results

3.1 CRISPR genome-wide screen

3.1.1 Cas9 stable expression and lentivirus mGeCKO library

To identify genes whose loss of function leads to OV resistance I performed a genome-wide CRISPR screen in the L1210 cell line. First, I characterized the susceptibility of the wildtype L1210 cell line to MG1-GFP infection *in vitro,* to ensure this cell line could be used in a screen for determining mechanisms of resistance. Increasing MOI correlated with decreasing metabolic activity, but by 43 hours post infection, all the tested MOIs showed no significant differences and the cells were extremely susceptible to MG1-GFP-induced cytotoxicity (Fig. 3A). Once infectivity was determined, L1210 cells were transduced with a lentivirus containing the Cas9 gene and selected with blasticidin. Clonal cell populations were derived from bulk Cas9 expressing cells by isolating single cells through flow cytometry and expanding in culture before cell lysates were tested for Cas9 expression by immunoblot (Fig. 3B). The growth of cells expressing Cas9 was not significantly altered from wildtype L1210 cells before 7 days of culture (Fig. 3C). The functionality of the Cas9 enzyme was tested by transducing clonal cells with lentiviruses containing gRNAs targeting essential genes, with the most efficiently functioning enzyme found in clone Cas9C (Fig. 3D). I also ensured that the stably-expressing Cas9 cell line could still be infected by MG1-GFP, no differently from wildtype L1210 cells. Differences in metabolic activity were only present at 24 hours after infection at MOI 0.1, but were abrogated at higher MOIs and altogether by 48 hours (Fig. 3E & 3F). Clonal cell line Cas9C showed not only the highest protein expression and no effect on MG1-GFP infectivity after 48 hours, but also

the greatest functional effect *in vitro,* without altering cell growth and was, therefore, selected to be used for all subsequent screening.

The murine GeCKO library was amplified from DNA plasmid stock in *E. coli* bacteria and transfected along with packaging plasmids in order to generate infectious lentiviral particles. The complete library was separated in two halves, A and B, each comprising about 65,000 gRNAs. Different volumes of the lentivirus library were then transduced onto the same number of L1210 cells and selected with puromycin, to determine the ratio required for a desired percent viability following selection (Fig. 3G). Following viability analysis by flow cytometry, the ratio of lentivirus library stock volume and cell number was determined in order to achieve approximately 30% viability of cells after antibiotic selection.

A genome-wide screen identifying means of resistance to OV infection might be limited to previously known anti-viral mechanisms such as the type I IFN pathway. To ensure that L1210 cells and their susceptibility to OV were not inadvertently affected by exposure to type I IFN, I pre-treated L1210 cells with type I IFN, followed by MG1-GFP infection at an MOI of 0.1. Cells seemed to respond to type I IFN alone by increasing metabolic activity and perhaps proliferation. However, after allowing enough time for virus-induced cytotoxicity to appear, all infected cells, regardless of previous exposure to type I IFN, displayed susceptibility with no significant differences between infected samples (Fig. 3H). This indicated that L1210 cells were not impacted by the associated antiviral effects of type I IFN.

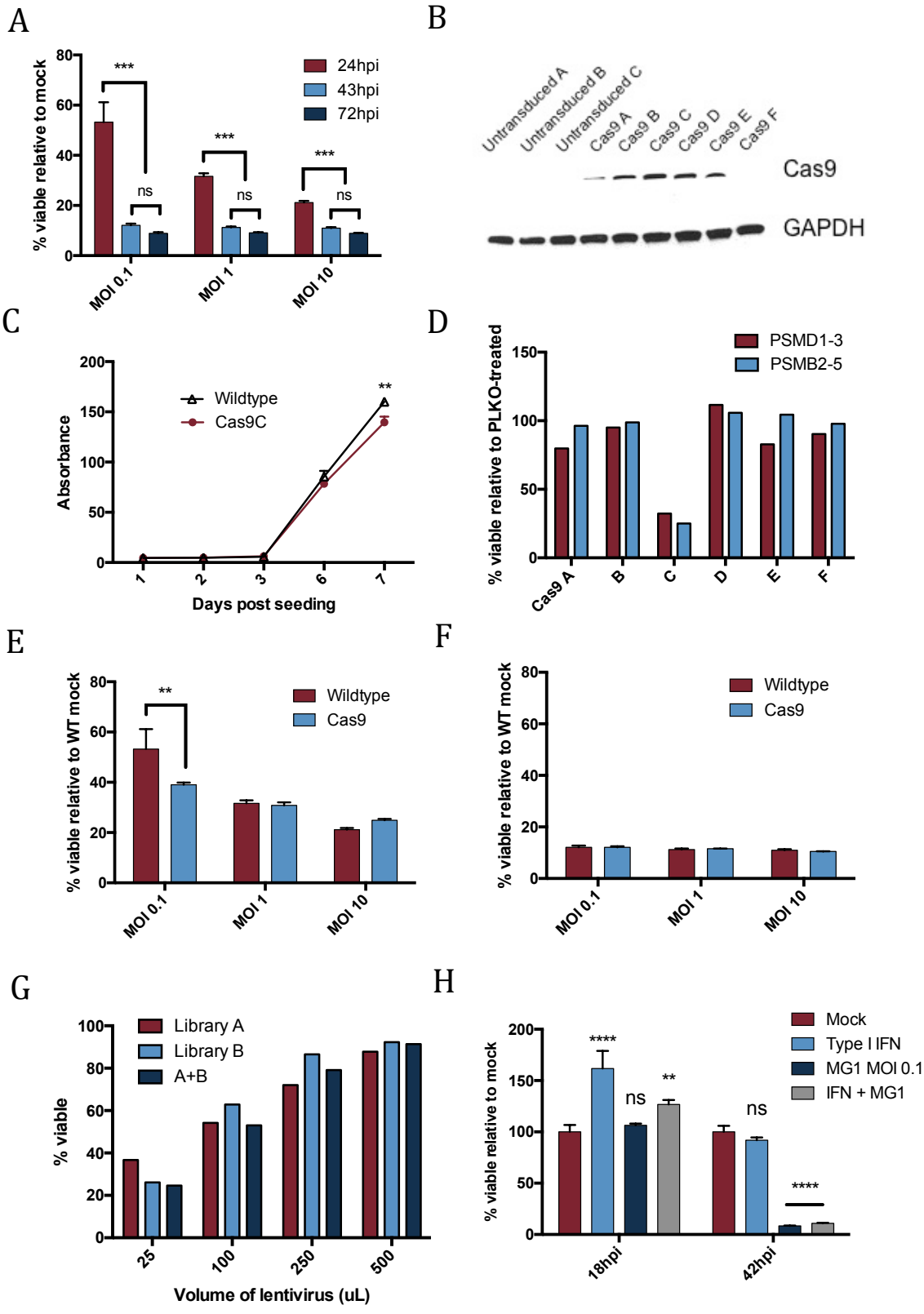
A
% viable relative to mock
24hpi
43hpi
72hpi
***
ns
MOI 0.1
MOI 1
MOI 10
B
Untransduced A
Untransduced B
Untransduced C
Cas9 A
Cas9 B
Cas9 C
Cas9 D
Cas9 E
Cas9 F
Cas9
GAPDH
C
Absorbance
Wildtype
Cas9C
**
Days post seeding
D
% viable relative to PLKO-treated
PSMD1-3
PSMB2-5
Cas9 A
B
C
D
E
F
E
% viable relative to WT mock
Wildtype
Cas9
**
MOI 0.1
MOI 1
MOI 10
F
% viable relative to WT mock
Wildtype
Cas9
MOI 0.1
MOI 1
MOI 10
G
% viable
Library A
Library B
A+B
25
100
250
500
Volume of lentivirus (uL)
H
% viable relative to mock
Mock
Type I IFN
MG1 MOI 0.1
IFN + MG1
****
ns
**
ns
****
18hpi
42hpi

Figure 3. Production and validation of CRISPR screen components. A. Infection of wildtype L1210 cells with MG1-GFP at MOIs 0.1, 1 and 10. Resazurin assay measured metabolic activity/viability at 24, 43 and 72 hours post infection. **B.** Immunoblot of lysates collected from clonal L1210 cells transduced with lentivirus containing *Cas9* gene. Untransduced cells had no exposure to the *Cas9* lentivirus. GAPDH was stained as a housekeeping reference protein. **C.** Cell growth of the clonal L1210-Cas9C cell line compared to wildtype L1210 cells was measured by resazurin assay over 7 days after seeding in a 96-well plate. **D.** Clonal cell lines expressing Cas9 were transduced with a lentivirus containing a gRNA targeting one of two essentials genes *PSMD1* or *PSMB2* to assess Cas9 enzyme functionality. Cell viability was assessed through resazurin assay relative to control lentivirus PLKO-transduced cells. **E.** Wildtype or Cas9-expressing L1210 cells (clone C) were infected with MG1-GFP at an MOI of either 0.1, 1 or 10.. Resazurin assay measured cell viability after 24 after infection. **F.** The same experiment from **E**. was evaluated by an additional resazurin assay 48 hours post infection. **G.** 1e6 L1210 cells were transduced with different volumes of lentiviral stock of either single or combined halves of the murine GeCKO CRISPR library. Cells were selected with 4μg/mL of puromycin for 5 days and percent viability was measured by flow cytometry. **H.** L1210 cells were mock-infected, treated with universal type I IFN at 50U/ml for 4.5h, infected with MG1-GFP at an MOI of 0.1, or treated with IFN at 50U/mL for 4.5h and infected with MG1-GFP at MOI 0.1. A resazurin assay was performed 18 and 42 hours post infection. A 2-way ANOVA with Sidak's multiple comparison test was used for (C) and (E), and Tukey's multiple comparison test against mock-treated samples for (H).

3.1.2 Screen selection and cell viability

The CRISPR screen was performed in L1210 cells stably expressing Cas9 (clone C) by transducing the lentivirus mGeCKO library at an MOI of 0.3 and selecting for transduced cells with puromycin. Viability by flow cytometry of library-transduced cells was expectedly close to 30%, seeing as the desired MOI after selection was 0.3 (Fig. 4A).

Initially, as expected, MG1-GFP infection caused widespread cell death, even of library transduced cells. Viability was monitored by trypan blue exclusion until cell suspension regained higher percentage viability compared to mock replicates (Fig. 4B).

Lastly, to confirm cells were in fact resistant to MG1 infection, 99 days following the primary infection, surviving cells were re-infected with MG1-GFP. L1210 cells expressing Cas9 enzyme and library transduced mock-infected samples were all still extremely susceptible to OV-mediated cell death, whereas all library samples that were previously infected 99 days earlier showed no significant decrease in viability following a secondary infection, indicating these cells had acquired resistance to MG1 (Fig. 4C).

A

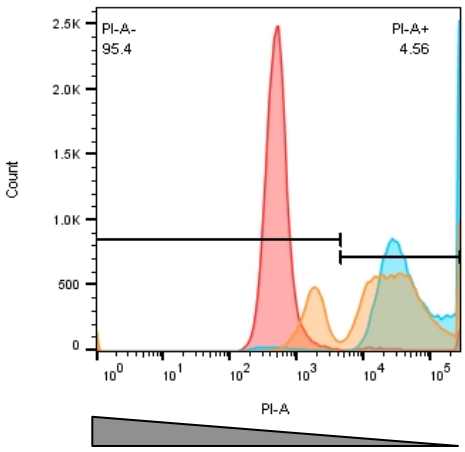

	Percent viable
Untransduced	95.4%
Puromycin control	3.7%
Library transduced	24.6%

Viability

B

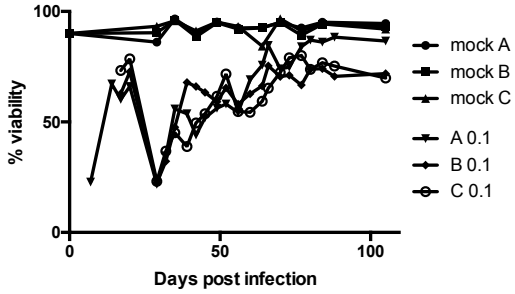

C

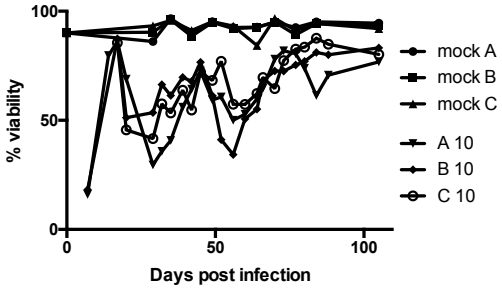

D

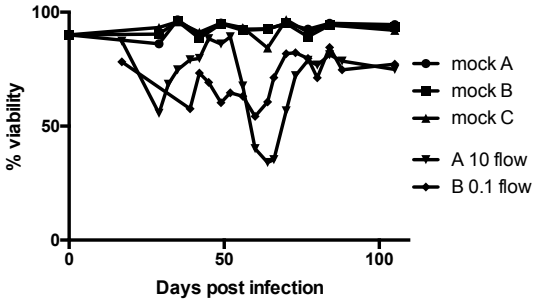

E

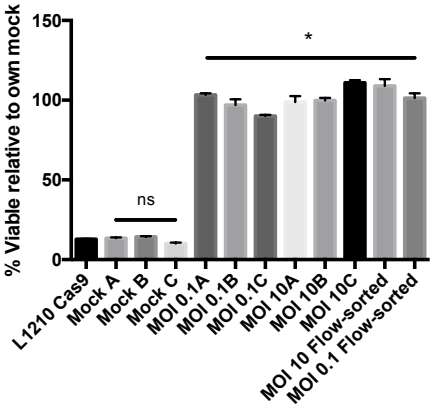

Figure 4. CRISPR screen cell viability and infection resistance. A. 1e6 of untransduced control cells, puromycin treated cells, or library-transduced and puromycin treated cells were stained with ethidium homodimer-1 at 0.1%v/v and analyzed for viability by flow cytometry. Cell aliquots from screen mock and infected samples were analyzed by trypan blue exclusion over the timecourse of the screen for MOIs 0.1 (**B**), 10 (**C**) and flow-sorted replicates (**D**). **E.** Cell samples from the screen were infected with MG1-GFP at an MOI of 1, 99 days after the initial infection. Metabolic activity was measured by resazurin assay 40 hours after infection. Each sample was analyzed relative to its own mock treatment. Statistics were performed using a one-way ANOVA with Sidak's multiple comparison test against Cas9-expressing cells.

3.1.3 Illumina next generation sequencing of CRISPR screen samples

Deep sequencing of DNA from library samples as well as cell samples from T29 and T117 (days after completed antibiotic selection), MOIs 0.1 and 10, and replicates were analyzed. First, read counts were normalized to reads per million (rpm) values. 92.6% of gRNAs were identified in the library plasmid sample. Guide RNAs with zero reads in all samples were removed; leaving 87.6% present in the cell library after transduction and selection (T0). The gRNA read count distribution was analyzed in the T0 sample as shown in Figure 5A. The overall read depth was lower than expected with a mean count of 473 rpm, and a median of 276 rpm, which is represented by the shape of the curve in Figure 5, however a few gRNAs had skewed over-representation, which was also found in the library plasmid sequenced sample. The read counts in each sample over time are depicted in Figure 5B. As expected with an enrichment screen, the expression of a cohort of gRNAs increased over time (particularly noticeable in T29 infected samples). The over-represented gRNAs present in the library persisted throughout the screen and are clearly visible in this plot .

A

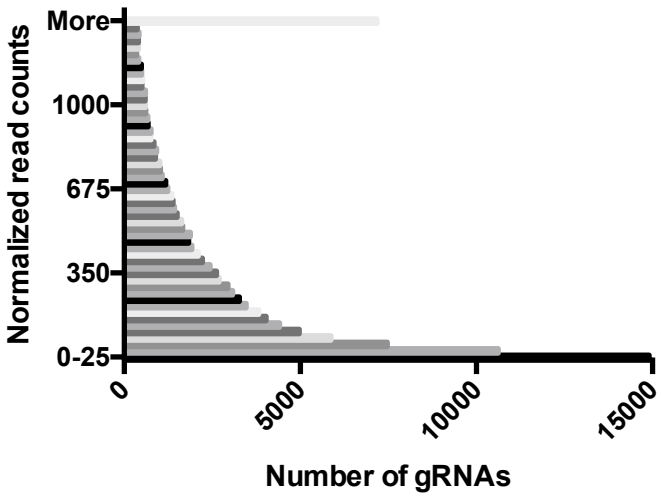
Normalized read counts
More
1000
675
350
0-25
0
5000
10000
15000
Number of gRNAs

B

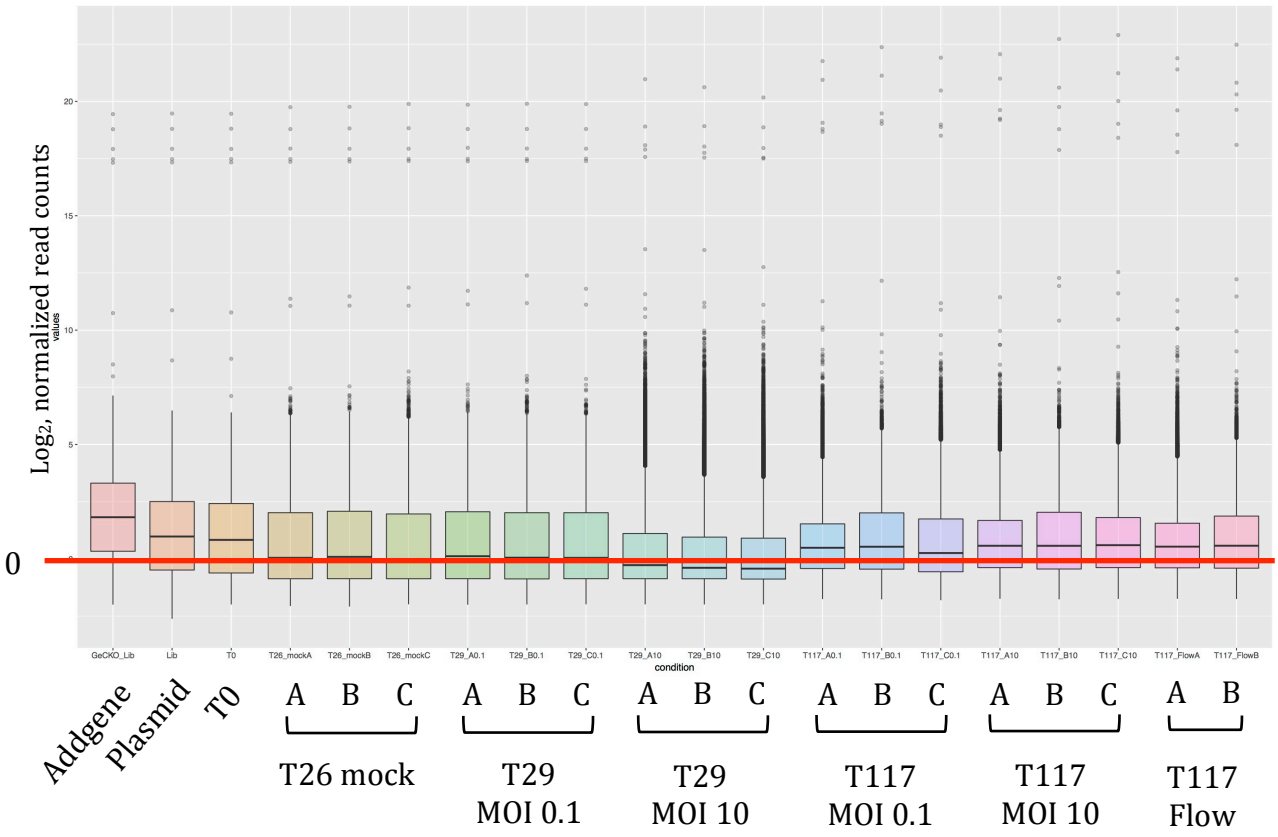
Log2, normalized read counts
values
0
20
15
10
5
GeCKO_Lib
Lib
T0
T26_mockA
T26_mockB
T26_mockC
T29_A0.1
T29_B0.1
T29_C0.1
T29_A10
T29_B10
T29_C10
T117_A0.1
T117_B0.1
T117_C0.1
T117_A10
T117_B10
T117_C10
T117_FlowA
T117_FlowB
condition
Addgene Plasmid
T0
A B C
T26 mock
A B C
T29 MOI 0.1
A B C
T29 MOI 10
A B C
T117 MOI 0.1
A B C
T117 MOI 10
A B
T117 Flow

Figure 5. Library gRNA read count distribution. A. The number of gRNAs in the sample T0 (0 days after selection was completed) plotted against their normalized read counts values. Read counts were normalized per million. **B.** gRNA library representation as normalized read counts (per million) for all timepoints and replicates on a Log_2 scale. Library representation was determined from Addgene provided FASTQ files of the mouse CRISPR knockout pooled library mGeCKOv2. Each sample is outlined by days after antibiotic selection was completed. Each triplicate is represented by A, B, or C, and MOI is detailed as either 0.1 or 10. Box plots represent data in quartiles with the middle line being the median and whiskers extend 1.5x the interquartile range. Outliers are shown as individual data points. Plots were generated using rlog transformation in DESeq2.

During analysis, mock and infected samples were separated by timepoint, either T29 (29 days after selection) or T117. gRNAs with zero reads across all mock and infected replicates at each timepoint were removed prior to analysis. At this point, 97.2% of gRNAs were expressed at T29, which decreased to 82.1% at T117. Lastly, in an attempt to reduce false positives, any gRNAs with expression in only one of the mock triplicates were removed from the analysis. From then, 65.7% of gRNAs expressed at T29 continued into further analysis, and 54% of the gRNAs expressed at T117 were analyzed (63.8% and 44.3% of the total gRNA library plasmid expression).

The MAGeCK test function was used to identify genes significantly enriched in MG1 treated samples relative to mock controls at each timepoint. Significantly enriched genes were identified as those ranked in the top 1% with at least 2 gRNAs meeting MAGeCK's requirements for a good gRNA. T29 analysis identified 129 genes at MOI 0.1 and 113 at MOI 10 under these criteria. T117 saw 16 genes at MOI 0.1 and 9 at MOI 10. 12 genes were sorted from analyzing flow-sorted samples at T117.

The summaries of significantly enriched genes for each timepoint were then aligned to identify the most prominent genes mediating resistance to MG1. Sixteen genes were identified across multiple samples, with many having some previously known link to virus infection. These findings are listed in Table 1, along with how many times they were identified in different samples and/or replicates and how many sequenced gRNAs were identified as significantly enriched in infected samples relative to mock controls. Nine unique genes were found to be potentially biologically relevant. The read counts for each gRNA in mock and virus treated samples at T29 and T117 at MOI 0.1 are shown in Figure. 6.

All genes identified as significantly enriched in at least two replicates, with the exception of *Ldlr*, were identified as significant in either the early or the late timepoint analyzed, but not both. Since an outlier gRNA may affect an otherwise overall trend per sample, and not all of the sequenced gRNAs showed a fold change in expression, I analyzed top hit genes with functional relevance at T29 or T117, either including all expressed gRNAs (Fig 7A and B), or only those gRNAs that were identified as enriched in infected samples (Fig 7C and D).

Table 1. Significant screen findings.

Gene	Sample timepoints identified as enriched	MOI replicates identified as enriched (Yes = Y or No =N)			Maximum identified number of significantly enriched gRNAs (max possible=6) per sample
		0.1	10	Flow	
Ldlr	T29	Y	Y		4
	T117	Y	Y	Y	
Filip1	T117	Y			2
Tmod4	T117	Y			3
Atp6v1g2	T29	Y	Y		3
Cav1	T29	Y	Y		2
Atg5	T29	Y	Y		2
Olfr1257	T29	Y	Y		2
Rhd	T29	Y	Y		3
Adam10	T29	Y	Y		3
Atf3	T29	Y	Y		5
Itga4	T29	Y	Y		2
Plau	T117	Y			2
Rfpl4	T117	Y			2
Tspan2	T117	Y			2
Tpr	T117			Y	3
2010109I03Rik or Ly6m	T117		Y		2

A T29 MOI 0.1

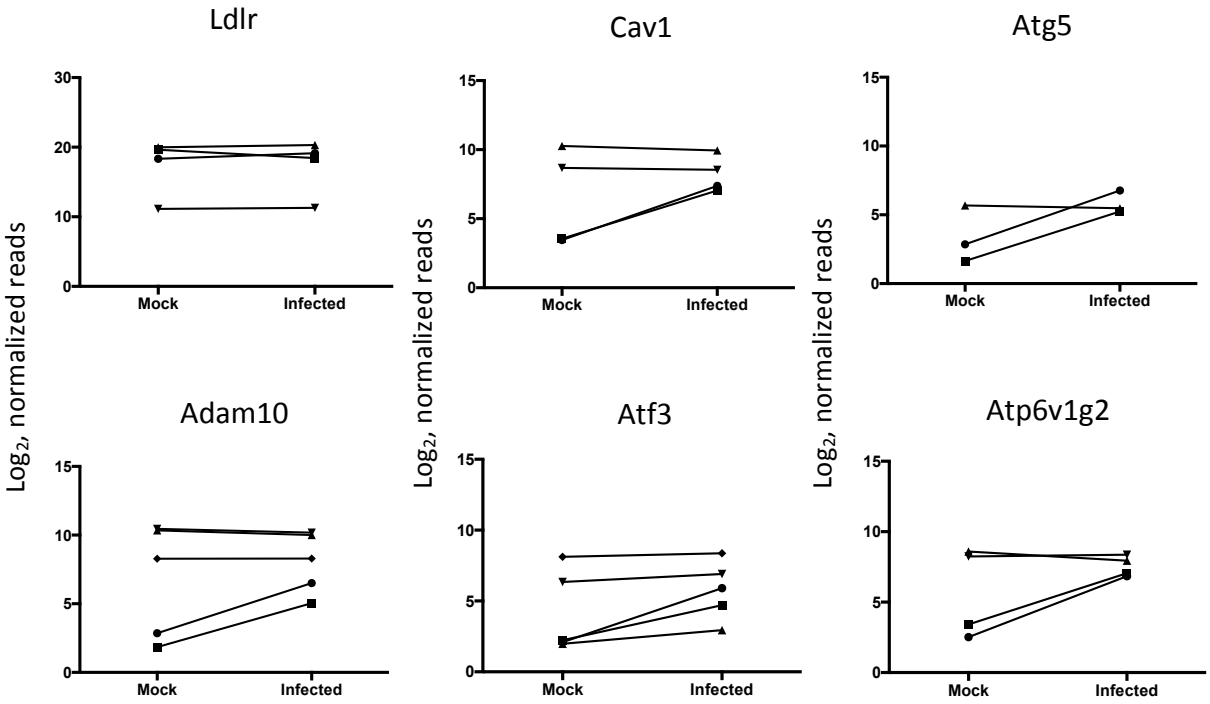

B T117 MOI 0.1

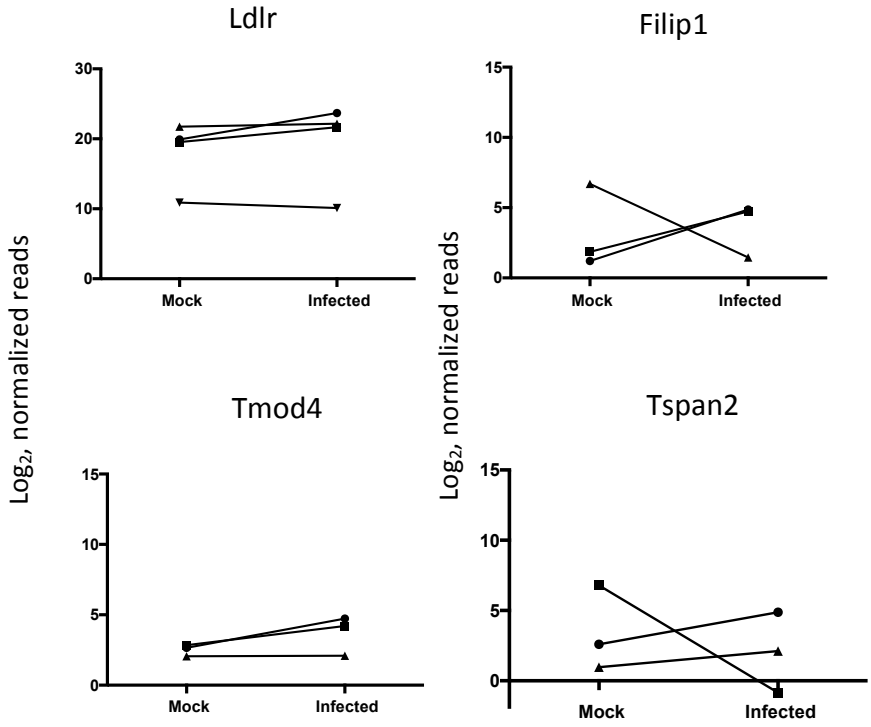

Figure 6. Expression of gRNAs in mock-treated and infected screen samples. Each gene that was identified as a top hit for the screen overall, with possible functional connections to viral susceptibility is included. All gRNAs identified as enriched in T29 **(A)** or T117 **(B)** samples at an MOI of 0.1 are plotted by normalized read counts, per million, on a Log2 scale. Mock-treated samples were collected on T26 and T96, and correlated to infected samples from T29 or T117, respectively.

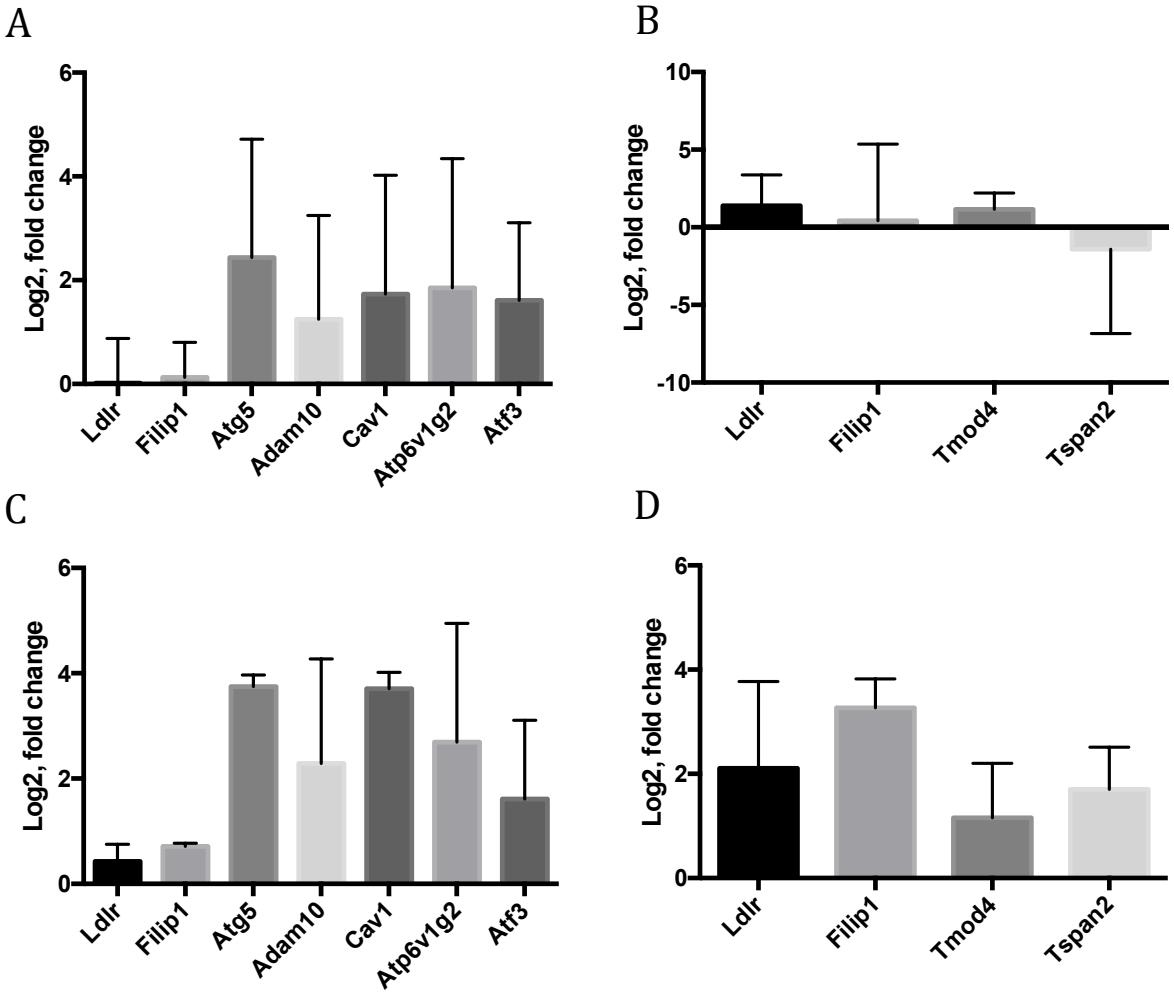
A
Log2, fold change
6
4
2
0
Ldlr
Filip1
Atg5
Adam10
Cav1
Atp6v1g2
Atf3
B
Log2, fold change
10
5
0
-5
-10
Ldlr
Filip1
Tmod4
Tspan2
C
Log2, fold change
6
4
2
0
Ldlr
Filip1
Atg5
Adam10
Cav1
Atp6v1g2
Atf3
D
Log2, fold change
6
4
2
0
Ldlr
Filip1
Tmod4
Tspan2

Figure 7. Fold change of gRNAs in infected samples. Fold change of gRNA read counts on a Log2 scale for significantly enriched genes at each timepoint at MOI 0.1 with at least 2 enriched gRNAs. All expressed gRNAs are included for either T29 (**A**) or T117 (**B**) followed by only enriched gRNAs for T29 (**C**) or T117 (**D**).

3.2 LDL receptor knockout

3.2.1 LDL-receptor knockout impairs in vitro *infection*

To generate an L1210 murine ALL cell line with greater resistance to OV infection, I worked towards creating a loss of function mutation in the LDL receptor, a top hit identified in the CRISPR screen. It has been previously shown that without access to a transmembrane member of the LDL-R family, both VSV and MG1 rhabdoviruses cannot infect cells, demonstrating that my screen identified genes that would be expected. Clonal cell populations transduced with a single *Ldlr* gRNA in the lentiGuide-Puro backbone were single cell sorted by flow cytometry and expanded individually in culture. Protein lysates were collected and analyzed through immunoblot, where two clonal cell populations were identified to have complete loss of protein expression, clone 2 and 8 (Fig. 8A). Loss of *Ldlr* expression was confirmed by Sanger sequencing in both clones, with clone 2 harbouring an 8 base pair deletion and clone 8, a 5 base pair deletion in the *Ldlr* sequence (Fig. 8B). Evaluation of growth characteristics by rezasurin assay, showed that neither clone's growth was impaired relative to parental controls. In fact, both clones had modestly increased metabolic activity, albeit not significant (Fig. 8C).

The two validated LDL-R knockout (KO) L1210 cell lines were then tested *in vitro* to determine if KO impaired MG1-GFP infection and altered viability relative to LDL-R expressing controls at multiple MOIs. The resazurin assay showed that a significantly higher number of *Ldlr* knockout cells were still viable 24, 48 and 72 hrs (Fig. 9 A-C) after OV infection, indicating that KO does in fact mediate resistance. This was also observed by fluorescence microscopy (EVOS), in which KO cells showed

reduced fluorescence compared to controls (Fig. 9D & 9E). Interestingly, at 48hrs post infection, *Ldlr* KO cells showed increased fluorescence compared to the same samples at 24hrs post infection. While the KO cells were still clearly more resistant than cells expressing *Ldlr*, these findings suggest that the virus is gaining entry into these cells via another receptor- likely an *Ldlr* family member, but that this receptor is far less efficient.

A

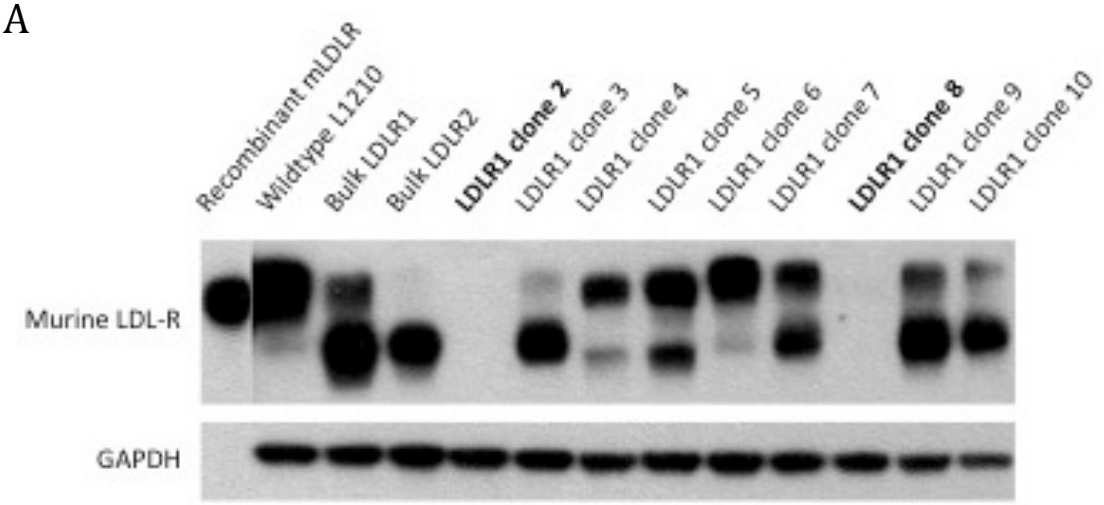
Recombinant mLDLR
Wildtype L1210
Bulk LDLR1
Bulk LDLR2
LDLR1 clone 2
LDLR1 clone 3
LDLR1 clone 4
LDLR1 clone 5
LDLR1 clone 6
LDLR1 clone 7
LDLR1 clone 8
LDLR1 clone 9
LDLR1 clone 10
Murine LDL-R
GAPDH

B

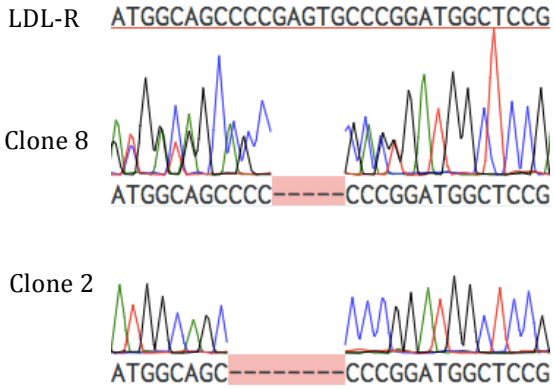
LDL-R
ATGGCAGCCCCGAGTGCCCGGATGGCTCCG
Clone 8
ATGGCAGCCCC-----CCCGGATGGCTCCG
Clone 2
ATGGCAGC--------CCCGGATGGCTCCG

C

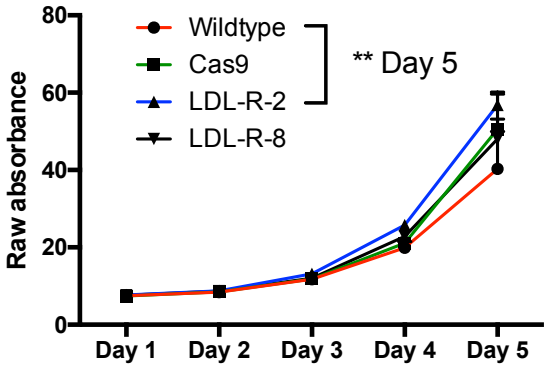
Wildtype
Cas9
LDL-R-2
LDL-R-8
** Day 5
Raw absorbance
80
60
40
20
0
Day 1
Day 2
Day 3
Day 4
Day 5

Figure 8. Generation of LDL receptor knockout L1210 cells. A. L1210 cells were transduced with lentiGuide-Puro vector containing a gRNA targeting LDL receptor and lysates from clonally selected transduced cells were isolated and run on an SDS-PAGE gel. PVDF-transferred membranes were stained with primary antibodies against murine LDL receptor and GAPDH proteins. **B.** Clones 2 and 8 were Sanger sequenced and analyzed against the referenced gene sequence. **C.** Clones 2 and 8 were compared with wildtype and Cas9-expressing L1210 cells regarding cell growth over 5 days using resazurin assay. A two-way ANOVA was done with Tukey's multiple comparisons test.

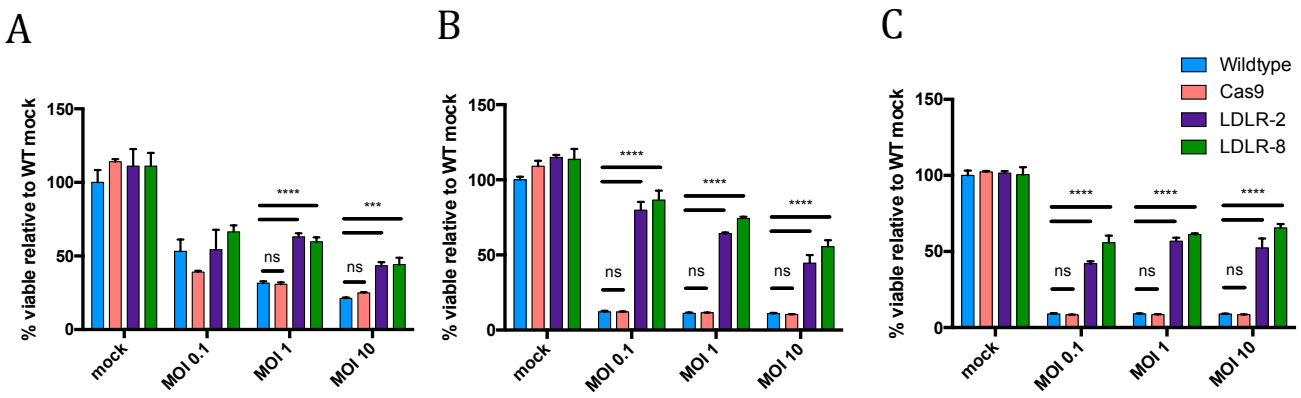
A
B
C
% viable relative to WT mock
150
100
50
0
mock
MOI 0.1
MOI 1
MOI 10
ns
****
***
Wildtype
Cas9
LDLR-2
LDLR-8

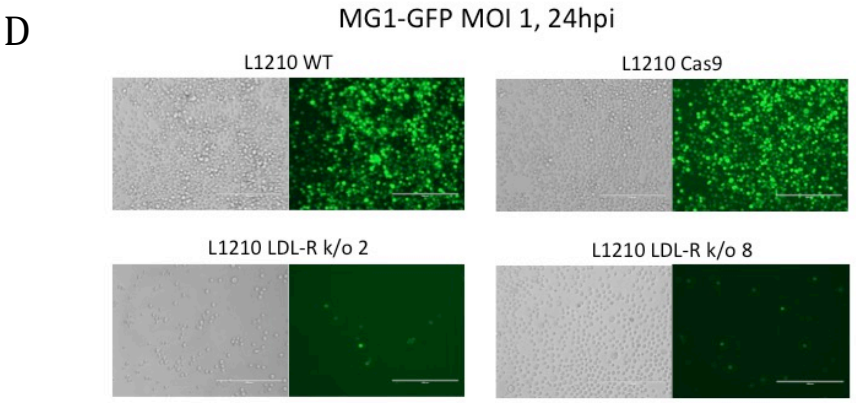
D
MG1-GFP MOI 1, 24hpi
L1210 WT
L1210 Cas9
L1210 LDL-R k/o 2
L1210 LDL-R k/o 8

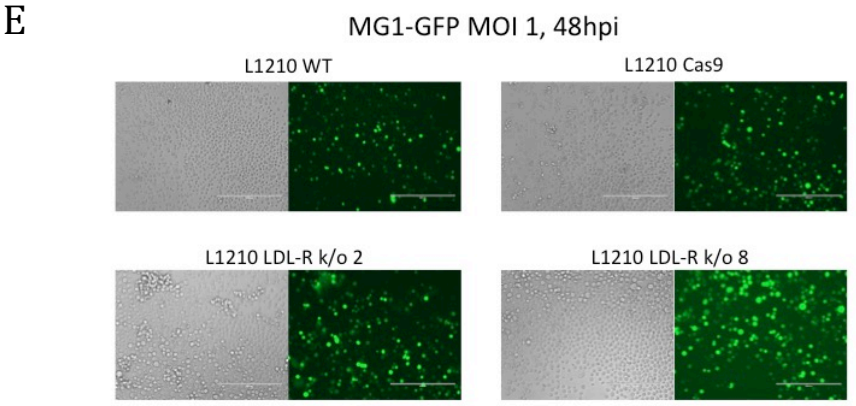
E
MG1-GFP MOI 1, 48hpi
L1210 WT
L1210 Cas9
L1210 LDL-R k/o 2
L1210 LDL-R k/o 8

Figure 9. LDL receptor facilitates *in vitro* MG1-GFP infection. L1210 cells containing loss of function mutations in LDL receptor (clones 2 and 8), or expressing Cas9 were infected with MG1-GFP at MOIs 0.1, 1, or 10 to determine virus susceptibility compared to wildtype cells. A resazurin assay was performed at 24 (**A**), 43 (**B**), and 72 (**C**) hours post infection. **D.** Fluorescence microscopy images of the same cell lines infected with MG1-GFP at MOI 1 after 24 hours of infection, where WT = wildtype L1210 cells. **E.** Images of the same cell samples from (D), taken 48 hours post infection. Statistics were done using 2-way ANOVA and Tukey's multiple comparison tests.

3.2.2 In vivo *ICV prepared with LDL receptor knockout cells*

Given that my L1210 *Ldlr* KO cells impaired infection *in vitro*, I was interested in determining whether this resistance would impact the cells' ability to provide immunogenic protection in an ICV format, especially knowing that OV infection is critical for ICV efficacy. After receiving ICV vaccinations, mice were challenged twice with 1e6 viable wildtype cells injected IV, 43 days apart. All groups receiving ICV showed the same level of protection, regardless of which cell line was used to prepare them (Fig. 10). While LDL receptor delayed MG1-GFP transgene expression *in vitro*, it did not have a significant impact on ICV immunogenicity or survival after *in vivo* challenge.

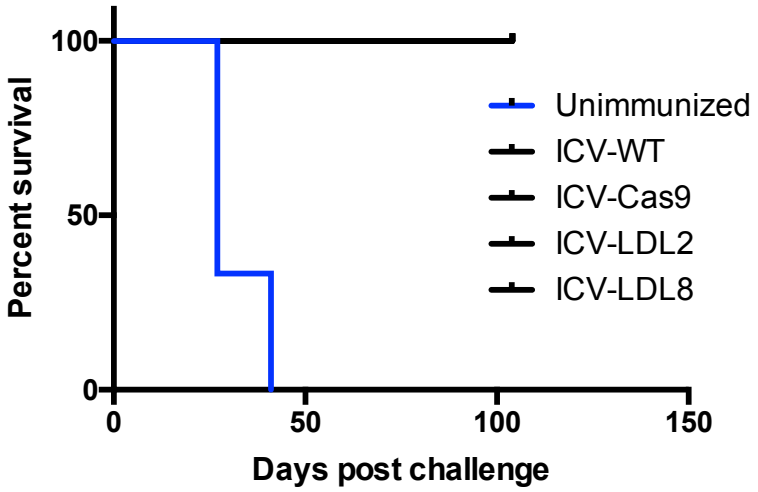
100
50
0
Percent survival
0
50
100
150
Days post challenge
Unimmunized
ICV-WT
ICV-Cas9
ICV-LDL2
ICV-LDL8

Figure 10. LDL-receptor knockout-ICV provides anti-leukemic protection. DBA/2 mice (n=3 per group) received ICV prepared from one of four different L1210 cell lines: wildtype (WT), Cas9-expressing (Cas9), LDL-R knockout clone 2 (LDL2) or LDL-R knockout clone 8 (LDL8). ICV was prepared by infecting cells at MOI 10 for 18 hours and γ-irradiating at 30 Gy. All groups except for unimmunized were injected with 3 doses of 1e6 ICV cells via tail vein per week for 3 weeks. A leukemic challenge was administered one week later as 1e6 viable L1210 cells to all mice. Mice then received a secondary challenge of another 1e6 viable cells 43 days after primary challenge. Kaplan-Meier survival plot is shown.

3.3 IV and SQ *in vivo* models of L1210 leukemia

3.3.1 SQ L1210 tumour growth characteristics

To identify if there are any differences between two models of L1210 leukemia in DBA/2 mice, I first characterized administration of SQ tumours with the murine ALL cell line and monitored tumour growth. Compared to an IV model of leukemia, where mice succumb to disease around 20 days after injection, a SQ model was not dissimilar (Fig. 11A). All mice grew tumours at every inoculation/implantation dose, with the lower injection dose growing slowest over time. Before 30 days, every animal grew a tumour greater than 15x15mm, which was the endpoint threshold, with many vastly exceeding this number by 15 days after challenge (Fig. 11B).

A

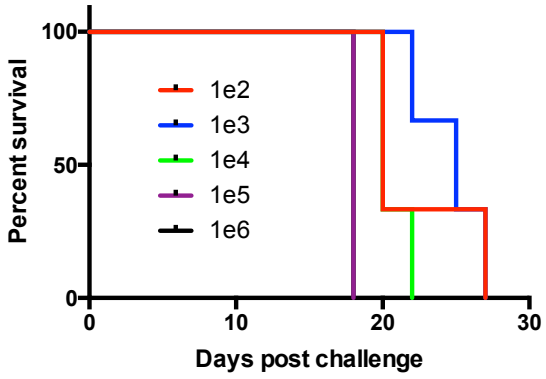
100
50
0
Percent survival
0
10
20
30
Days post challenge
1e2
1e3
1e4
1e5
1e6

B

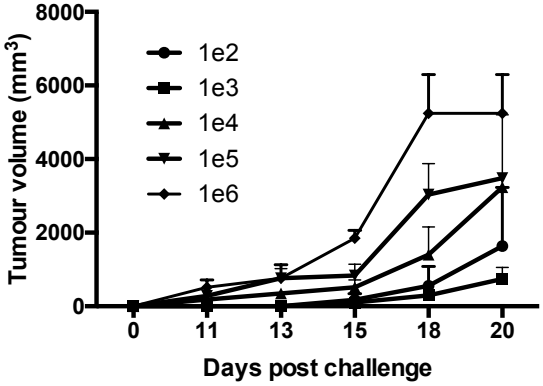
8000
6000
4000
2000
0
Tumour volume (mm3)
0
11
13
15
18
20
Days post challenge
1e2
1e3
1e4
1e5
1e6

Figure 11. Characterization of subcutaneous L1210 tumours. A. Survival of DBA/2 mice subcutaneously injected with 1e2 to 1e6 viable L1210 cells in the right flank (n=3). **B.** Volumes of SQ L1210 tumours in the same mice up to 20 days after injection.

3.3.2 IV vs. SQ L1210 localization

I also investigated the localization of L1210 tumour cells in a head to head comparison of IV and SQ models. Leukemia is known to travel in circulation and home to bone marrow, spleen, lymph nodes[77], so I investigated tumour cell presence in the peripheral blood and the bone marrow using Giemsa staining. Blood and leg bones were collected from mice at endpoint for each tumour model. Blood was smeared onto slides and bone marrow was either dabbed directly onto slides, or isolated from the bone and smeared onto slides. Giemsa staining allowed for visualization of blast cells by staining nuclei a dark blue and cytoplasm, pink. Although a solid tumour mass was only present consistently in a SQ model, both administration routes of leukemia resulted in circulating lymphoblasts, as well as a vast amount of homing to the bone marrow (Fig. 12 A-D).

A

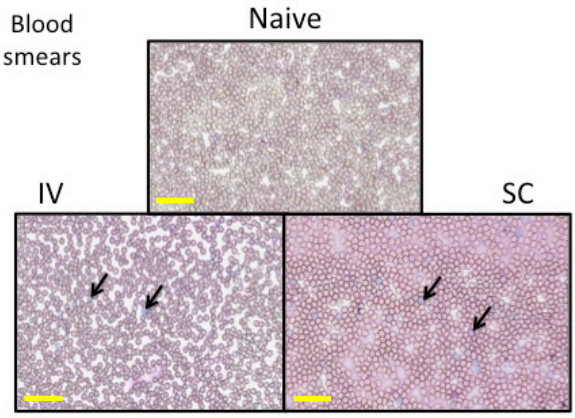
Blood
smears
Naive
IV
SC

B

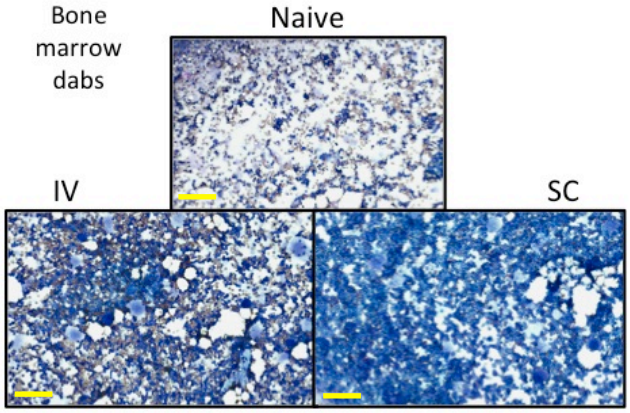
Bone
marrow
dabs
Naive
IV
SC

C

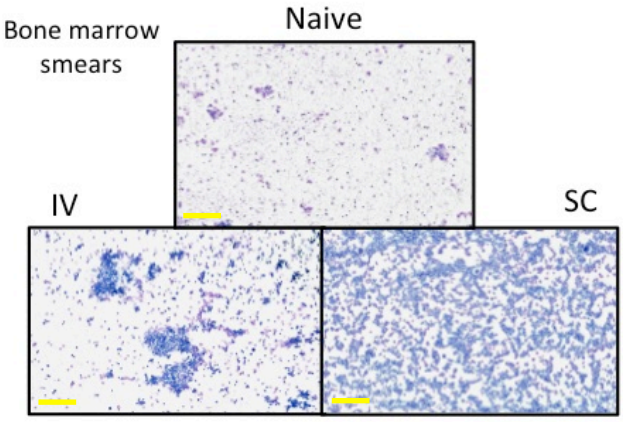
Bone marrow
smears
Naive
IV
SC

D

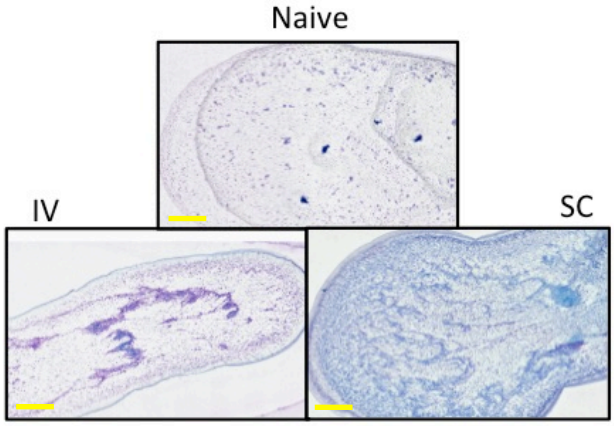
Naive
IV
SC

Figure 12. Localization of L1210 tumour cells in SQ and IV models. A. Blood smears of samples from naïve mice, or mice injected with L1210 cells SQ or IV, at endpoint. Smears were visualized with Giemsa-Wright stain at 50x magnification. Scale bars in yellow are 40μm. **B.** Marrow from femur or tibia bones was dabbed directly onto slides from the same endpoint mice; L1210 naïve, SQ, or IV challenged. Giemsa-Wright stain was used on slides and magnified to 20x. Each scale bar is 100μm. **C.** Giemsa-wright stain was performed again, but on diluted smears of harvested bone marrow, also from femur or tibia bones from endpoint mice. Pictures were taken at 10x and scale bars represent 200μm. **D.** Bone marrow smear samples from C. were visualized at magnification 2x with scale bars at 1mm.

3.3.3 ICV protection of IV vs. SQ L1210 tumours

Seeing as an ICV dosing regimen can protect against an IV L1210 tumour, I sought to determine if the same was true for SQ tumours, and if so, whether the threshold of protection was the same. From previous experiments, it was determined that the ICV-protected threshold challenge dose for IV tumours is 1e6 cells. While the tumour cells circulate and home similarly in both models, the solid tumour mass could be a major roadblock for the immune response. ICV was administered to mice three times, once a week, followed by a tumour challenge at different doses for each group (n=3). Initially, I investigated small dose differences around the 1e6 cell midpoint. Only one mouse in the lower 5e5 cell challenge group survived (Fig. 13A), leading me to repeat this experiment using additional lower tumour challenge doses to find which dose would provide 100% protection. Upon completing this experiment, it appeared that a 1e5 cell challenge was protected and all mice survived long term (Fig. 13B). All other groups with lower tumour challenge doses also survived over 100 days after challenge. Without immunization, SQ implanted tumours grew to an endpoint volume by 30 days after challenge, however their growth was delayed in ICV immunized mice by an additional 10-20 days. This is not the case for IV implanted tumours, where leukemic advancement and endpoint are not delayed at an unprotected challenge dose.

A

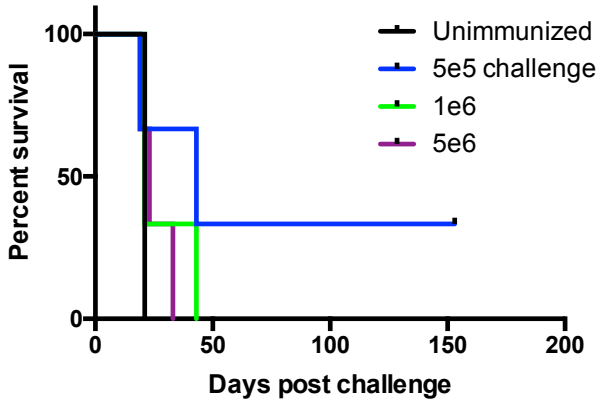
Percent survival
100
50
0
0
50
100
150
200
Days post challenge
Unimmunized
5e5 challenge
1e6
5e6

B

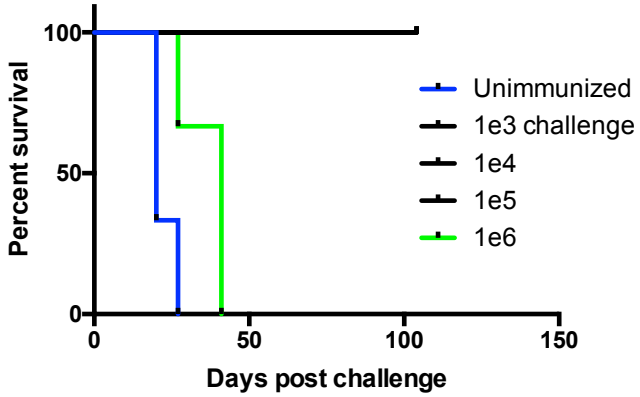
Percent survival
100
50
0
0
50
100
150
Days post challenge
Unimmunized
1e3 challenge
1e4
1e5
1e6

Figure 13. ICV vaccination protects against SQ L1210 challenge. A. DBA/2 mice were vaccinated with ICV prepared from L1210 cells and MG1-GFP infection 3 times weekly, before receiving a SQ challenge of viable L1210 cells at varying doses between 5e5 and 1e6 viable cells (n=3). **B.** DBA/2 mice were again ICV vaccinated 3 times weekly, followed by SQ challenge of viable L1210 cells at a larger dose range from 1e3 to 1e6 viable cells (n=3).

Chapter 4: Discussion

4.1 Interpreting the CRISPR genome-wide screen results

4.1.1 gRNA representation

Although 92.6% (120,574 gRNAs) of the 130,209 gRNAs in the mGeCKOv2 library were expressed in our library preparation, indicating that plasmid amplification and creation of lentiviral stocks was successful, we obtained lower gRNA representation than expected due to reduced sequencing depth. This was observed across all samples and directly impacted the number of guides identified in each sample, as well as the accuracy of their representation, however, as this was an enrichment screen it should not have impaired our ability to detect gRNAs enriched in virus infected samples. The box plots in Figure 5B, show a slightly higher read count distribution of guides in the plasmid library sequence data provided by Addgene, which is due to a greater sequencing depth. Regardless, gRNAs were identified in all samples and the average and median reads per gRNA in the T0 cell sample was 473 and 296 rpm, respectively.

Interestingly, we also observed a small number of gRNAs ($n<10$) that were highly over-represented in all samples we sequenced (Fig. 5). Importantly, we were able to show that these same gRNAs are highly enriched in the reference plasmid library file provided by Addgene, suggesting it is an inherent issue with the plasmid library and not due to manipulation in our hands. The presence of these gRNAs in later timepoints and infected samples suggested that resistance to MG1-GFP infection was conferred. If a gRNA was expressed and did not alter the susceptibility of the cell to MG1-GFP, the cell would be exposed to virus during the screen and have undergone

virus-mediated cytotoxicity, leading to the elimination of that gRNA from the cell population, no matter how abundant it may have originally been. Therefore, while a large fold change may not occur, its continued presence in infected cell samples suggests a gRNA and its associated target played a role in the viral life cycle.

The box plots in Figure 5B contain lots of valuable information about the screen. First, the gRNA representation from T0 was largely maintained in mock-treated samples at T26 as was expected. The decrease in expression of some gRNAs is due to the loss of gRNAs targeting genes essential for cell survival. MG1-GFP infected samples also saw an overall drop in the number of gRNAs expressed, which was an additional expected result of the treatment because wildtype L1210 cells are extremely susceptible to virus infection. Most cells and their corresponding expressed gRNAs were eliminated from the screen, unless the conferred mutation impacted cell survival following virus exposure. The first look at infected samples at T29 demonstrated an increase in outlier gRNAs, indicating these samples were undergoing selection. This trend continued in later timepoints across all infected samples. It is true that this effect could be seen modestly in early mock samples at T26, perhaps due to the possiblility that some gRNAs were being selected for due to their effects on cell proliferation and survival. A gRNA that created a mutation, and conferred a growth advantage to a cell population, may have increased in representation compared to other gRNA-expressing cells. While this may seem like a confounding factor, all infected samples were analyzed and compared to their corresponding mock-treated samples from a very similar time in the screen experiment. Mock samples from T26 were used as control samples for T29

infected cells. Similarly, T96 mock-treated cells were controls for T117 infected samples. Therefore, all fold changes in gRNA expression took this effect into account.

4.1.2 Top gene results

Following analysis with the MAGeCK software, which was specifically designed to analyze CRISPR screen data, 16 genes were identified as significantly enriched in virus treated samples in at least 2 conditions (MOI and time). Of these genes, 9 had known function that could potentially influence virus infection and susceptibility. Most of the genes were identified in early timepoints of the screen, as seen in the gRNA expression increases and fold changes at T29 in Figures 6 and 7. Two of the genes identified in the MOI 0.1 early timepoint screens remained significant at the later T117 timepoints, namely *Ldlr* and *Filip1*. However, the other findings at T29 show great potential for their role in virus infection despite the loss of a fold change later on, including *Cav1*, *Atg5*, and *Adam10*, for example. Regardless of their functional potential a future direction preceding all others is validation of these findings. One way to achieve this would be through siRNA knockdown of genes followed by MG1 infection and assessing the effect of each knockdown on viral infectivity, replication and titer. These experiments may be followed by mechanistic investigations, generating CRISPR knockouts of genes for further research or ICV experiments, for example.

4.1.2.1 Ldlr

The most likely finding of this screen, based on previous work assessing rhabdovirus infection, is the identification of *Ldlr*. *Ldlr* has been identified not only as a binding receptor for LDL, but also as a receptor that mediates VSVΔ51 and MG1 entry[38,39]. The LDL-R protein is a major viral receptor and its loss leads to decreased

infection[38]. Moreover, the LDL-R protein family can all act in this fashion, and complete inhibition of this family of proteins leads to a total block in viral entry[61]. Therefore, it was expected to be included in the list of genes whose loss of function would increase cellular resistance to MG1-GFP. Increasing expression of LDL-R or its protein family members would be one method to increasing infection levels, however, this may also increase the tropism of the virus and lead to more off-target effects. Selectively achieving this effect could improve infection of tumour cells and OV therapy, by for instance, targeted delivery of plasmid-encoding LDL-R or upstream pathway activation. While it was identified in the CRISPR screen and increased cellular resistance to OV infection in this setting, the effects of LDL-R are not crucial to completely abrogating infection *in vitro*, and its expression is not required when generating an immunogenic ICV with MG1-GFP (Figures 9 & 10 and section 4.2). That being said, these results do not rule out the possibility that LDL-R protein over-expression may provide the desired, opposite effect of increasing cellular susceptibility and improving infection in otherwise more resistant cells.

4.1.2.2 Caveolin-1

The early timepoint screening results identified a number of genes that were significantly enriched following MG1-GFP OV infection. Caveolin-1 is a protein known to form part of the coating structure of caveolae where it acts as a lipid binding adapter protein[78,79]. In addition, non-caveolar caveolin-1 regulates a number of pathways including signal transduction and vesicular transport, one of which is the MEK/ERK pathway[79,80]. Depending on the cellular status and the context of pathway activation, caveolin-1 may lead to extracellular signal regulated kinase (ERK) activation through

interaction with kinase suppressor of Ras 1 (KSR1)[80]. KSR1 is an important regulator of growth factor-induced ERK activation to modulate cell proliferation among other pathway outcomes, and caveolin-1 is required for this effect[80]. The MEK/ERK pathway has been exploited by a number of viruses in order to facilitate infection, such as vaccinia, influenza B and rabies viruses-a member of the rhabdoviridae family to which MG1 also belongs[81–83]. These interactions suggest a positive correlation between pathway activation and productive virus infection. Further evidence supporting a link between caveolin-1, the MEK/ERK pathway and viral infection are two direct examples of caveolin-1 being employed in infected cells. A study investigating the replicative cycle of the paramyxovirus, parainfluenza virus 5 suggested a role for caveolin-1 in assembly and/or budding of enveloped virus particles, where lack of its expression led to maintained viral entry but reduced infectivity[84]. Caveolin-1 was also investigated for its role in Dengue virus infection, where it was found to possibly hold interactions with non-structural viral proteins and play an important part in both polyprotein processing and viral particle release[85]. It seems that caveolin-1 can play many roles in a number of processes, and virus infection is one of them. Viruses may have evolved mechanisms to directly interact with host proteins like caveolin-1, but it also may be implicated in pathways required for virus infection, cell proliferation, and viral assembly/release. Therefore, OV infection may be improved by recruitment of caveolin-1 and the activation of assisting pathways. A study done in uterine smooth muscle indicated that a reduction of membrane caveolin-1 occurred with 17β-estradiol estrogen treatment, which was prevented with progesterone and reversed with pure estrogen receptor antagonist[86]. The intracellular location may be affected by these treatments and could

be used as a way to alter its involvement in virus infection and assembly. Lastly, the MEK/ERK pathway can be negatively regulated at many stages, which provides many opportunities to promote pathway activation[87]. Whether through small molecule inhibitors, small interfering RNAs (siRNA) or OVs encoding micro RNA (miRNA), negative regulators of the pathway like Sprouty[88,89], dual-specificity MAP kinase phosphatases (Dusp or MKP)[90], or vaccinia H1-related (VHR)[91] proteins may be targeted and blocked in order to promote ERK activation and productive OV infection.

4.1.2.3 Atg5 and Atp6v1g2

Another gene with particularly interesting function as it may relate to virus infection is *Atg5*. Autophagy protein 5 (Atg5) is required in the homeostatic process of autophagy, which is a cell survival mechanism that aids in the removal of damaged organelles and misfolded proteins through lysosomal degradation, but its de-regulation can also lead to autophagic cell death[92]. Atg5 is known to form complexes with Atg12 and Atg16 and act like an E3 ubiquitin ligase enzyme to promote the conjugation between Atg8 and phosphatidylethanolamine, leading to downstream autophagosomal membrane development[93,94]. The functions of Atg5 extend beyond autophagy, with additional roles that are relevant to both OV infection and immunotherapy. For instance, this protein and the autophagic process is required for efficient T and B lymphocyte development, proliferation and survival[95,96]. Atg5 is also important for the development of mature natural killer (NK) cells and subsets of innate lymphoid cells[97]. Along the same lines of immune cell function, Atg5 is required for processing antigens for MHC II presentation in dendritic cells (DCs)[98]. An infected cell, whether an immune cell or not, could benefit from a functioning autophagy pathway as this could prolong

cell survival long enough for mature virions to release, as well as perhaps improved antigen processing for immune cell recognition. Directly related to virus replication, is its role in negatively regulating the type I IFN antiviral response. The Atg5-Atg12 complex was found to suppress and regulate signaling mediated by immunostimulatory RNA, including virus-derived or double-stranded RNA, by direct association with RIG-I and IPS-1, therefore contributing to RNA virus replication[99]. Lastly, Atg5 is involved in exosome production and vesicular transport by decreasing acidification of late endosomes[100]. During this process it removes a regulatory component of the vacuolar (V)-ATPase, ATP6V1E1, into exosomes, promoting their production and migration[100]. This was shown to promote cell migration and metastasis in an orthotopic model of breast cancer, but it is also important to note that exosomes can be useful for selectively delivering anti-tumour agents such as miRNAs[101]. Aiding in their production, cancer cells typically have upregulated production of these vesicles, which could be beneficial following viral infection for the delivery of therapeutic cargo[102,103].

At the same time as aiding with exosome formation, the V-ATPase is, more generally, involved in other intracellular acidification processes like protein sorting and receptor-mediated endocytosis, both of which could be connected to processes utilized by OVs upon infection[104]. Another component of this pathway, *Atp6v1g2,* was also identified as a top hit in the screen. This protein forms a subunit of the V-ATPase enzyme complex. Since rhabdoviruses like VSV, which is genetically very similar to MG1, use pH-dependent endocytosis for endosomal membrane fusion, the control of intracellular compartment acidity is an important tool for the virus to exploit[40]. In fact, it was determined previously that inhibition of the V-ATPase proton pump at a

concentration that abrogated the acidity of intracellular compartments, inhibited entry of VSV and transport of viral proteins, hence further validating the identification of a V-ATPase component in our screen[105].

Taking the many functions of Atg5 into consideration and the potentially linked effects of Atp6v1g2, these screen findings may be worth further investigating. Atg5 activity has many potential benefits for immunotherapies, such as promoting the development and survival of immune cell populations, as well as MHC presentation. In cancer cells that respond to type I IFN, an active Atg5-Atg12 complex could inhibit this pathway in order to promote OV infection. The role that Atg5 has on promoting vesicle formation in the form of exosomes may extrapolate to aiding with the configuration of mature virions, but also could be used to exploit the cargo-carrying capabilities of cancer-derived exosomes. In order to fully benefit from its potential, the expression and activation of Atg5 can be stimulated by targeting any negative regulators such as CNOT2[106]. Simultaneously, its actions can be therapeutically useful when it comes to targeted exosome therapy, especially when delivered by OV infection, in addition to its positive effects on promoting anti-tumour immunity. It would be very interesting to assess the role of Atg5 in the context of these therapies, first, by identifying its role during *in vitro* infection, followed by subsequent experiments regarding its additional immune-related functions. The effects on generating an anti-tumour immune response could be evaluated by targeting Atg5 in the L1210 ICV model. Finally, its impact on exosome production could be identified in various models *in vitro* and *in vivo* in the context of targeted exosome OV therapy, for example.

4.1.3 Other genes identified by the CRISPR screen

Several other genes with functionally relevant roles to OV infection were also identified by our screen. Filamin-A interacting protein 1 (Filip1), identified in early and late timepoints of the screen, promotes the degradation of filamin A. As a binding protein, filamin A crosslinks actin filaments and serves as a scaffold between the actin cytoskeleton and many cellular proteins. According to one study it was also associated with inactive RNase L, which otherwise interacted with filamin A to inhibit virus entry[107]. Cells lacking filamin A showed enhanced entry of virus[107], perhaps explaining why the lack of expression of a filamin A negative regulator would inhibit virus infection. There have been several components of the cytoskeleton linked to the importance of OV infection, and while Filip1 has not previously been identified as important for viral susceptibility, other cytoskeletal elements have been. For example, myxoma oncolytic virus was made more infectious in a model of breast cancer by inhibiting regulators of cortical actin structures, further suggesting a role for cytoskeletal elements to modulate virus susceptibility[108]. Another study found microtubules and their stabilization were important for cell susceptibility to virus infection[109]. Perhaps Filip1 can be connected to viral susceptibility/resistance in the same fashion.

A disintegrin and metalloprotease 10 (Adam10) is a cell surface protein that may have a role in virus infection as highlighted by a study regarding human immunodeficiency virus type-1 (HIV1). Silencing the expression of Adam10 resulted in inhibited HIV-1 replication, which the authors explain may have been due to a disruption at the level of nuclear trafficking[110]. If this effect extends to trafficking of

different proteins across the nuclear membrane, then it could possibly relate to the rhabdovirus matrix protein trafficking, or even other host proteins involved in virus replication.

The cAMP responsive element-binding (CREB) protein family of transcription factors which includes activating transcription factor 3 (Atf3), is part of the endoplasmic reticulum (ER) stress response pathway and promotes apoptotic cell death upon stress. The CREB transcription factor family has also been shown to promote activity and transcriptional induction of viral promoters, as shown for hepatitis B virus[111]. Components of the ER stress response have also been identified as synthetic lethal targets with Maraba infection in several cancer models, suggesting Atf3 and this pathway could play a role in mediating susceptibility/resistance to infection[112].

Less is known about the transmembrane protein tetraspanin 2 (Tspan2), but in a model of lung cancer it was responsible for cell motility and invasiveness and its only other known role is involving oligodendrocyte development[113,114]. It is also known to interact with other tetraspanins, CD9 and CD81[114]. The protein family have more detailed functions related to cell fusion and motility, infection, and cancer cell metastasis[114]. They are also highly enriched in exosomal membranes and are considered by some to be markers of exosomes[115].

Tropomodulin 4 (Tmod4) is a protein whose function blocks the elongation and depolymerization of actin filaments. Similar to Filip1 and filamin 1, interactions with actin, Tmod4 is involved in the regulation of the cell cytoskeleton. Perhaps a link can be drawn between these results and previous studies that identified other cytoskeletal elements were important for cell susceptibility to virus infection, as discussed above.

4.2 The impact of an LDL receptor knockout

When LDL-R was knocked out of the murine L1210 ALL cell line, it was expected that the susceptibility to rhabdovirus infection would be impaired due to previous work supporting this effect. Knowing that all members of the LDL receptor protein family can serve as binding proteins for VSV and MG1 entry, it was not unexpected that there was still some level of MG1-GFP infection in the *Ldlr* KO cells, albeit less than wildtype cells. While expression of viral proteins, as measured by green fluorescence within cells, occurred in fewer LDL-R knockout cells 24 hours post infection compared to wildtype controls, it appeared to be a delayed effect. Virus transgene expression increased in LDL-R knockout cells after 48 hours of infection based on increasing green fluorescence, although substantially less than wildtype cells, at the same time as fluorescence decreased in wildtype controls due to a decrease in cell viability. However, based on appearance, LDL-R knockout cells at this timepoint were still large, round and viable, whereas LDL-R wildtype cells had shrunken down and were not metabolically active. As measured by resazurin assay, metabolic activity remained comparably high in LDL-R knockout cells even 72 hours post infection. The delayed fluorescence in LDL-R knockout cells may be due to a lower ratio of available binding proteins on the cell surface. LDL-R is not the only protein member of its family, and others can take the place of LDL-R, also facilitating some level of infection in its absence[38]. If these alternate mechanisms of entry take time to facilitate infection, perhaps most cells were infected from the next generation of viral progeny, explaining the delayed fluorescence. Seeing as most LDL-R knockout cells in culture remained viable 72 hours after infection, even with increasing green fluorescence, it is unclear why the overall timeline of infection

seemed slower. In contrast, almost all wildtype cells showed cytotoxic effects from the virus after 43 hours of exposure regardless of the infected MOI. However, further experiments with these cell lines could elucidate the alternative mechanisms of viral binding used and changes in the infection timeline.

Since these cell lines did show significantly more metabolic activity and therefore, viability after MG1-GFP infection, I aimed to investigate whether the increased resistance would translate to less efficacious ICV. The effects *in vivo* were modest when incorporating these cell lines into an ICV. MG1 infection was impaired *in vitro* in LDL-R knockout cells, but it has previously been shown that an L1210 ICV with a very low ratio of infected cells can maintain its protective effects[54]. Therefore, if that infection ratio is equal to or greater than what was seen in an LDL-R knockout cell line, presumably an injected ICV formulated with these cells would still protect mice. Given that the level of fluorescence and infection in cells increased over time *in vitro* and that a large proportion of cells do become metabolically inactive, there would still be a significant proportion of virus-infected and unviable cells after a certain time. Again, this information leads me to believe that it was not unexpected for an ICV prepared using a cell line with reduced susceptibility to OV infection to still protect mice from leukemic challenge *in vivo*.

This data suggests that the ICV is dependent on OV infection, but, as predicted, only a small number of infected cells are required for its protection. It is promising to know this information because cancer cells with even greater resistance to virus infection could still benefit from ICVs. However, between different models there are most likely other aspects impacting efficacy and survival in addition to virus resistance.

Cancers that are severely resistant to rhabdovirus infection could be at a large disadvantage when it comes to ICV therapy, because some level of infection is required for its efficacy based on the leukemic model. Therefore, it is still worthwhile to investigate mechanisms of viral resistance in cancer cells, to not only create a better understanding, but also to improve direct virus-mediated cytotoxicity as well as other OV-based therapies, of which ICV is included. The results of an LDL-R knockout in this cell line are also worth investigating further. Seeing that infection occurred, although less than when exposed to wildtype L1210 cells, but at a delayed rate is an interesting phenomenon. It is possible that the virus is utilizing alternative methods of binding to the cell surface in order to facilitate entry, which perhaps may be slower. The kinetics of the two infection conditions could be investigated by collecting viral titers and protein expression data over the course of an experiment. It might also be interesting to confirm whether other methods of entry are possible, by inhibiting binding to all of the LDL-R protein family members, in order to determine if any receptor-independent methods of viral entry are employed. Overall, the level of infection was significantly lower in cells without LDL-R expression, however, the change in infection kinetics despite this reduction of virus would be interesting to pursue.

4.3 Differences in models of L1210 leukemia

A SQ model of an otherwise systemic, liquid tumour was investigated for its feasibility in DBA/2 mice, as well as to what extent an ICV would protect against these tumours compared to their non-solid counterparts. Tumours grew to endpoint condition at relatively the same rate, and cells migrated systemically to the bone marrow in both groups, with a solid flank tumour forming in only the SQ injected

animals. While the tumours grew quickly in both models and circulated similarly, I was interested in whether or not an ICV made with the same L1210 tumour cells would protect mice from a SQ challenge just as it does for an IV challenge. At the same challenge dose for protection in an IV model, the SQ tumours persisted and grew to endpoint, although delayed relative to untreated controls. At a slightly lower dose of 1e5 cells instead of 1e6, all the mice challenged with a flank tumour survived and had no visible signs of solid tumour mass. In between at 5e5 cells, one mouse survived long term after SQ challenge. A lower protective challenge dose was predicted for a SQ leukemia model seeing as the ICV functions by mounting an anti-leukemia immune response. The cells responsible for inducing this response circulate systemically and through lymphoid organs and are attracted to areas with specific antigen recognition, drawn in by other molecules such as chemokines. The circulating and homing tumour cells in an IV mouse model rarely take shape as a large, solid tumour mass, as is the case for SQ. Perhaps the immune cells have easier, internal access to IV injected tumour cells because of their location in the animal. A SQ tumour is isolated from systemic circulation at first, and there is a better chance for the cells to form a network and a very different kind of tumour microenvironment, where lack of access and immunosuppression could play larger roles. Overall, these aspects have not been shown in this particular model yet, but the results of our ICV experiments suggest this may be the case.

Although the Giemsa-stained images of bone marrow seem to show enhanced homing of tumour cells in the SQ model of disease, this could be due to differential tumour cell migration and homing between the two models. Based on previous murine

studies, an IV model of leukemia may also show an abundance of cancerous cells proliferating and homing in other organs such as the spleen and lymph nodes[77,116–118]. This was not investigated during my experiments, but it could explain the similar survival rates and disease effects while looking solely at blood and bone marrow samples.

There are several reasons to consider a solid tumour leukemic model but first, the largest disadvantage is the lack of translation to human cases of ALL, because these cancers simply do not naturally develop in this SQ fashion. However, in the lab, it can allow for easier access to tumour cells for downstream analysis at the same time as providing a helpful visual aid in assessing tumour burden and progression. Using this model, manipulation of tumour cells is made easier and intratumoural therapies can also be investigated. Overall, a solid tumour model of leukemia could prove very useful in research and may be able to serve other questions in future experiments.

Chapter 5: Conclusions

A number of genes were identified from a CRISPR genome-wide screen assessing how loss of function mutations promote resistance to MG1-GFP infection. Loss of function of LDL receptor, Caveolin-1, Atg5, Atp6v1g2, Filip1, Adam10, Tmod4, Tspan2, and Atf3 were all identified as top screen findings with known function that could be correlated to cell susceptibility to virus infection.

LDL receptor is an important but not exclusive binding receptor that facilitates rhabdovirus, and specifically MG1, infection. Loss of its expression reduces the level of infection, and may also delay its occurrence. Expression of LDL-R is not required for sufficient MG1-GFP infection in an L1210 ICV leukemia model to protect mice from subsequent tumour challenge.

The L1210 leukemia DBA/2 mouse model behaves differently when injected subcutaneously or intravenously. A solid tumour only consistently forms from a SQ injection, allowing for tumour progression to be recorded and visualized. Both models of injection find tumour cells homing to femur and tibia bone marrow. The two models follow a similar timeline of disease progression until endpoint, where the aggressive nature of the tumour kills mice typically before 30 days when administered above a certain injection threshold. An infected cell vaccine protects all mice that received a lower challenge dose (1e5 cells) in SQ injected animals compared to IV injected mice (1e6). ICV may prolong the survival of mice with SQ-injected tumours below the threshold of protection, but does not in an IV model.

Bibliography

1. Canadian Cancer Society. Canadian Cancer Statistics 2017. *Can. Cancer Soc.* **2017,** 1–132 (2017).
2. Dores, G. M., Devesa, S. S., Curtis, R. E., Linet, M. S. & Morton, L. M. Acute leukemia incidence and patient survival among children and adults in the United States, 2001-2007. *Blood* **119,** 34–43 (2012).
3. Leukemia and Lymphoma Society of Canada. Facts and Statistics: About Blood Cancers. *LLSCanada* Available at: http://www.llscanada.org/disease-information/facts-and-statistics. (Accessed: 19th April 2018)
4. Alvarnas, J. C. *et al.* Acute Lymphoblastic Leukemia, Version 2.2015. *J. Natl. Compr. Canc. Netw.* **13,** 1240–79 (2015).
5. Terwilliger, T. & Abdul-Hay, M. Acute lymphoblastic leukemia: a comprehensive review and 2017 update01. *Blood Cancer J.* **7,** e577 (2017).
6. Webert, K., Cook, R. J., Sigouin, C. S., Rebulla, P. & Heddle, N. M. The risk of bleeding in thrombocytopenic patients with acute myeloid leukemia. *Haematologica* **91,** 1530–7 (2006).
7. Ahmadzadeh, A. *et al.* Infection Pattern of Neutropenic Patients in Post-chemotherapy Phase of Acute Leukemia Treatment. *Hematol. Rep.* **5,** e15 (2013).
8. Rowe, J. M. Prognostic factors in adult acute lymphoblastic leukaemia. *Br. J. Haematol.* **150,** no-no (2010).
9. Liu-Dumlao, T., Kantarjian, H., Thomas, D. A., O'Brien, S. & Ravandi, F. Philadelphia-Positive Acute Lymphoblastic Leukemia: Current Treatment Options. *Curr. Oncol. Rep.* **14,** 387–394 (2012).
10. Bachanova, V. *et al.* Ph+ ALL patients in first complete remission have similar survival after reduced intensity and myeloablative allogeneic transplantation: impact of tyrosine kinase inhibitor and minimal residual disease. *Leukemia* **28,** 658–665 (2014).
11. Shimoni, A. *et al.* Long-term survival and late events after allogeneic stem cell transplantation from HLA-matched siblings for acute myeloid leukemia with myeloablative compared to reduced-intensity conditioning: a report on behalf of the acute leukemia working party of European group for blood and marrow transplantation. *J. Hematol. Oncol.* **9,** 118 (2016).
12. Achkar, W. Al, Wafa, A., Ali, B. Y., Manvelyan, M. & Liehr, T. A rare chronic myeloid leukemia case with Philadelphia chromosome, BCR-ABL e13a3 transcript and complex translocation involving four different chromosomes. *Oncol. Lett.* **1,** 797–800 (2010).
13. Deininger, M. *et al.* International Randomized Study of Interferon Vs STI571 (IRIS) 8-Year Follow up: Sustained Survival and Low Risk for Progression or Events in Patients with Newly Diagnosed Chronic Myeloid Leukemia in Chronic Phase (CML-CP) Treated with Imatinib. *Blood* **114,** (2009).

14. Ottmann, O. G. *et al.* A phase 2 study of imatinib in patients with relapsed or refractory Philadelphia chromosome-positive acute lymphoid leukemias. *Blood* **100,** 1965–1971 (2002).

15. Gleissner, B. *et al.* Leading prognostic relevance of the BCR-ABL translocation in adult acute B-lineage lymphoblastic leukemia: a prospective study of the German Multicenter Trial Group and confirmed polymerase chain reaction analysis. *Blood* **99,** 1536–43 (2002).

16. Leoni, V. & Biondi, A. Tyrosine kinase inhibitors in BCR-ABL positive acute lymphoblastic leukemia. *Haematologica* **100,** 295–9 (2015).

17. Ottmann, O. G. *et al.* Imatinib compared with chemotherapy as front-line treatment of elderly patients with Philadelphia chromosome-positive acute lymphoblastic leukemia (Ph+ALL). *Cancer* **109,** 2068–2076 (2007).

18. Tanguy-Schmidt, A. *et al.* Long-Term Follow-Up of the Imatinib GRAAPH-2003 Study in Newly Diagnosed Patients with De Novo Philadelphia Chromosome-Positive Acute Lymphoblastic Leukemia: A GRAALL Study. *Biol. Blood Marrow Transplant.* **19,** 150–155 (2013).

19. Otero, D. C. & Rickert, R. C. CD19 function in early and late B cell development. II. CD19 facilitates the pro-B/pre-B transition. *J. Immunol.* **171,** 5921–30 (2003).

20. Hartmann, J., Schüßler-Lenz, M., Bondanza, A. & Buchholz, C. J. Clinical development of CAR T cells-challenges and opportunities in translating innovative treatment concepts. *EMBO Mol. Med.* **9,** 1183–1197 (2017).

21. Kantarjian, H. *et al.* Blinatumomab versus Chemotherapy for Advanced Acute Lymphoblastic Leukemia. *N. Engl. J. Med.* **376,** 836–847 (2017).

22. Topp, M. S. *et al.* Long-term follow-up of hematologic relapse-free survival in a phase 2 study of blinatumomab in patients with MRD in B-lineage ALL. *Blood* **120,** 5185–5187 (2012).

23. Topp, M. S. *et al.* Safety and activity of blinatumomab for adult patients with relapsed or refractory B-precursor acute lymphoblastic leukaemia: a multicentre, single-arm, phase 2 study. *Lancet Oncol.* **16,** 57–66 (2015).

24. Topp, M. S. *et al.* Phase II Trial of the Anti-CD19 Bispecific T Cell–Engager Blinatumomab Shows Hematologic and Molecular Remissions in Patients With Relapsed or Refractory B-Precursor Acute Lymphoblastic Leukemia. *J. Clin. Oncol.* **32,** 4134–4140 (2014).

25. Shannon L. Maude, David T. Teachey, Susan R. Rheingold, Pamela A Shaw, Richard Aplenc, David Maxwell Barrett, Christine S Barker, Colleen Callahan, Noelle V. Frey, Farzana Nazimuddin, Simon F. Lacey, Zhaohui Zheng, Bruce Levine, Jan Joseph Melenhorst, Lau, S. A. G. Sustained remissions with CD19-specific chimeric antigen receptor (CAR)-modified T cells in children with relapsed/refractory ALL. *J. Clin. Oncol.* **34,** 3011–3011 (2016).

26. Ruella, M. & Maus, M. V. Catch me if you can: Leukemia Escape after CD19-Directed T Cell Immunotherapies. *Comput. Struct. Biotechnol. J.* **14,** 357–362

(2016).

27. Fitzgerald, J. C. *et al.* Cytokine Release Syndrome After Chimeric Antigen Receptor T Cell Therapy for Acute Lymphoblastic Leukemia. *Crit. Care Med.* **45,** e124–e131 (2017).

28. Chen, Y. *et al.* [The expression of CD19 in 210 cases of childhood acute leukemia and its significance]. *Zhonghua er ke za zhi = Chinese J. Pediatr.* **42,** 188–91 (2004).

29. Stojdl, D. F. *et al.* VSV strains with defects in their ability to shutdown innate immunity are potent systemic anti-cancer agents. *Cancer Cell* **4,** 263–75 (2003).

30. Kaufman, H. L. *et al.* Systemic versus local responses in melanoma patients treated with talimogene laherparepvec from a multi-institutional phase II study. *J. Immunother. Cancer* **4,** 12 (2016).

31. Brun, J. *et al.* Identification of genetically modified Maraba virus as an oncolytic rhabdovirus. *Mol. Ther.* **18,** 1440–9 (2010).

32. Chen, A. *et al.* Oncolytic measles virus enhances antitumour responses of adoptive CD8+NKG2D+ cells in hepatocellular carcinoma treatment. *Sci. Rep.* **7,** 5170 (2017).

33. Kim, S.-G. *et al.* Phase II trial of pexa-vec (pexastimogene devacirepvec; JX-594), an oncolytic and immunotherapeutic vaccinia virus, in patients with metastatic, refractory renal cell carcinoma (RCC). *J. Clin. Oncol.* **36,** 671–671 (2018).

34. Hughes, J. *et al.* Lister strain vaccinia virus with thymidine kinase gene deletion is a tractable platform for development of a new generation of oncolytic virus. *Gene Ther.* **22,** 476–484 (2015).

35. Ilett, E. *et al.* Prime-boost using separate oncolytic viruses in combination with checkpoint blockade improves anti-tumour therapy. *Gene Ther.* **24,** 21–30 (2017).

36. Ribas, A. *et al.* Oncolytic Virotherapy Promotes Intratumoral T Cell Infiltration and Improves Anti-PD-1 Immunotherapy. *Cell* **170,** 1109–1119.e10 (2017).

37. Regan, A. D. & Whittaker, G. R. in 167–177 (Springer, New York, NY, 2006). doi:10.1007/978-1-4614-7651-1_9

38. Finkelshtein, D., Werman, A., Novick, D., Barak, S. & Rubinstein, M. LDL receptor and its family members serve as the cellular receptors for vesicular stomatitis virus. *Proc. Natl. Acad. Sci.* **110,** 7306–7311 (2013).

39. Tong, J. G. *et al.* Spatial and temporal epithelial ovarian cancer cell heterogeneity impacts Maraba virus oncolytic potential. *BMC Cancer* **17,** 594 (2017).

40. Albertini, A. A. V, Baquero, E., Ferlin, A. & Gaudin, Y. Molecular and cellular aspects of rhabdovirus entry. *Viruses* **4,** 117–39 (2012).

41. Johannsdottir, H. K., Mancini, R., Kartenbeck, J., Amato, L. & Helenius, A. Host cell factors and functions involved in vesicular stomatitis virus entry. *J. Virol.* **83,**

440–53 (2009).

42. Sun, X., Yau, V. K., Briggs, B. J. & Whittaker, G. R. Role of clathrin-mediated endocytosis during vesicular stomatitis virus entry into host cells. *Virology* **338,** 53–60 (2005).

43. Banerjee, A. K. *Transcription and Replication of Rhabdoviruses*. *MICROBIOLOGICAL REVIEWS* **51,** (1987).

44. Jan, M. & Majeti, R. Clonal evolution of acute leukemia genomes. *Oncogene* **32,** 135–140 (2013).

45. Scott, A. M., Allison, J. P. & Wolchok, J. D. Monoclonal antibodies in cancer therapy. *Cancer Immun.* **12,** 14 (2012).

46. Hodi, F. S. *et al.* Improved Survival with Ipilimumab in Patients with Metastatic Melanoma. *N. Engl. J. Med.* **363,** 711–723 (2010).

47. Reck, M. *et al.* Pembrolizumab versus Chemotherapy for PD-L1–Positive Non–Small-Cell Lung Cancer. *N. Engl. J. Med.* **375,** 1823–1833 (2016).

48. Engeland, C. E. *et al.* CTLA-4 and PD-L1 checkpoint blockade enhances oncolytic measles virus therapy. *Mol. Ther.* **22,** 1949–59 (2014).

49. Wu, A. A., Drake, V., Huang, H.-S., Chiu, S. & Zheng, L. Reprogramming the tumor microenvironment: tumor-induced immunosuppressive factors paralyze T cells. *Oncoimmunology* **4,** e1016700 (2015).

50. Hanna, M. G. & Jr. Immunotherapy with autologous tumor cell vaccines for treatment of occult disease in early stage colon cancer. *Hum. Vaccin. Immunother.* **8,** 1156–60 (2012).

51. Filatenkov, A. *et al.* Ineffective vaccination against solid tumors can be enhanced by hematopoietic cell transplantation. *J. Immunol.* **183,** 7196–203 (2009).

52. Karcher, J. *et al.* Antitumor vaccination in patients with head and neck squamous cell carcinomas with autologous virus-modified tumor cells. *Cancer Res.* **64,** 8057–61 (2004).

53. Thind, K., Padrnos, L. J., Ramanathan, R. K. & Borad, M. J. Immunotherapy in pancreatic cancer treatment: a new frontier. *Therap. Adv. Gastroenterol.* **10,** 168–194 (2017).

54. Conrad, D. P. *et al.* Leukemia cell-rhabdovirus vaccine: personalized immunotherapy for acute lymphoblastic leukemia. *Clin. Cancer Res.* **19,** 3832–43 (2013).

55. Lemay, C. G. *et al.* Harnessing oncolytic virus-mediated antitumor immunity in an infected cell vaccine. *Mol. Ther.* **20,** 1791–9 (2012).

56. Stetson, D. B. & Medzhitov, R. Type I Interferons in Host Defense. *Immunity* **25,** 373–381 (2006).

57. Swiecki, M. & Colonna, M. Type I interferons: diversity of sources, production pathways and effects on immune responses. *Curr. Opin. Virol.* **1,** 463–75 (2011).

58. Ivashkiv, L. B. & Donlin, L. T. Regulation of type I interferon responses. *Nat. Rev. Immunol.* **14,** 36–49 (2014).

59. Hussain, M. M. Structural, biochemical and signaling properties of the low-density lipoprotein receptor gene family. *Front. Biosci.* **6,** D417-28 (2001).

60. Cureton, D. K., Massol, R. H., Saffarian, S., Kirchhausen, T. L. & Whelan, S. P. J. Vesicular stomatitis virus enters cells through vesicles incompletely coated with clathrin that depend upon actin for internalization. *PLoS Pathog.* **5,** e1000394 (2009).

61. Tong, J. G. *et al.* Evidence for differential viral oncolytic efficacy in an in vitro model of epithelial ovarian cancer metastasis. *Mol. Ther. oncolytics* **2,** 15013 (2015).

62. Barrangou, R. *et al.* CRISPR provides acquired resistance against viruses in prokaryotes. *Science* **315,** 1709–12 (2007).

63. Brouns, S. J. J. *et al.* Small CRISPR RNAs guide antiviral defense in prokaryotes. *Science* **321,** 960–4 (2008).

64. Jinek, M. *et al.* A programmable dual-RNA-guided DNA endonuclease in adaptive bacterial immunity. *Science* **337,** 816–21 (2012).

65. Doudna, J. A. & Charpentier, E. The new frontier of genome engineering with CRISPR-Cas9. *Science (80-.).* **346,** (2014).

66. Chen, S. *et al.* Genome-wide CRISPR Screen in a Mouse Model of Tumor Growth and Metastasis. *Cell* **160,** 1246–1260 (2015).

67. Marraffini, L. A. *The CRISPR-Cas system of Streptococcus pyogenes: function and applications*. *Streptococcus pyogenes: Basic Biology to Clinical Manifestations* (University of Oklahoma Health Sciences Center, 2016).

68. Kim, H. S. *et al.* CRISPR/Cas9-mediated gene knockout screens and target identification via whole-genome sequencing uncover host genes required for picornavirus infection. *J. Biol. Chem.* **292,** 10664–10671 (2017).

69. Sanjana, N. E., Shalem, O. & Zhang, F. Improved vectors and genome-wide libraries for CRISPR screening. *Nat. Methods* **11,** 783–784 (2014).

70. Mao, Z., Bozzella, M., Seluanov, A. & Gorbunova, V. DNA repair by nonhomologous end joining and homologous recombination during cell cycle in human cells. *Cell Cycle* **7,** 2902–6 (2008).

71. Su, T. *et al.* A CRISPR-Cas9 Assisted Non-Homologous End-Joining Strategy for One-step Engineering of Bacterial Genome. *Sci. Rep.* **6,** 37895 (2016).

72. Shalem, O. *et al.* Genome-scale CRISPR-Cas9 knockout screening in human cells. *Science* **343,** 84–87 (2014).

73. Hou, P. *et al.* A Genome-Wide CRISPR Screen Identifies Genes Critical for Resistance to FLT3 Inhibitor AC220. *Cancer Res.* **77,** 4402–4413 (2017).

74. Patel, S. J. *et al.* Identification of essential genes for cancer immunotherapy.

Nature **548,** 537–542 (2017).

75. Parnas, O. *et al.* A Genome-wide CRISPR Screen in Primary Immune Cells to Dissect Regulatory Networks. *Cell* **162,** 675–86 (2015).

76. CRISPR loss of function screening - Target Discovery Institute. *Nuffield Department of Medicine, University of Oxford* (2018). Available at: https://www.tdi.ox.ac.uk/crispr-loss-of-function-screening. (Accessed: 17th July 2018)

77. Gopalakrishnapillai, A. *et al.* Disruption of Annexin II /p11 Interaction Suppresses Leukemia Cell Binding, Homing and Engraftment, and Sensitizes the Leukemia Cells to Chemotherapy. *PLoS One* **10,** e0140564 (2015).

78. Anderson, R. G. W. THE CAVEOLAE MEMBRANE SYSTEM. *Annu. Rev. Biochem.* **67,** 199–225 (1998).

79. Smart, E. J. *et al.* Caveolins, liquid-ordered domains, and signal transduction. *Mol. Cell. Biol.* **19,** 7289–304 (1999).

80. Kortum, R. L. *et al.* Caveolin-1 Is Required for Kinase Suppressor of Ras 1 (KSR1)-Mediated Extracellular Signal-Regulated Kinase 1/2 Activation, H-RasV12-Induced Senescence, and Transformation. *Mol. Cell. Biol.* **34,** 3461–3472 (2014).

81. Ludwig, S. *et al.* MEK inhibition impairs influenza B virus propagation without emergence of resistant variants. *FEBS Lett.* **561,** 37–43 (2004).

82. Manjunatha, V. *et al.* Inhibition of MEK-ERK1/2-MAP kinase signalling pathway reduces rabies virus induced pathologies in mouse model. *Microb. Pathog.* **112,** 38–49 (2017).

83. Bonjardim, C. A. Viral exploitation of the MEK/ERK pathway – A tale of vaccinia virus and other viruses. *Virology* **507,** 267–275 (2017).

84. Ravid, D., Leser, G. P. & Lamb, R. A. A role for caveolin 1 in assembly and budding of the paramyxovirus parainfluenza virus 5. *J. Virol.* **84,** 9749–59 (2010).

85. García Cordero, J., León Juárez, M., González-Y-Merchand, J. A., Cedillo Barrón, L. & Gutiérrez Castañeda, B. Caveolin-1 in Lipid Rafts Interacts with Dengue Virus NS3 during Polyprotein Processing and Replication in HMEC-1 Cells. *PLoS One* **9,** e90704 (2014).

86. Turi, A., Kiss, A. L. & Müllner, N. Estrogen downregulates the number of caveolae and the level of caveolin in uterine smooth muscle. *Cell Biol. Int.* **25,** 785–794 (2001).

87. Lake, D., Corrêa, S. A. L. & Müller, J. Negative feedback regulation of the ERK1/2 MAPK pathway. *Cell. Mol. Life Sci.* **73,** 4397–4413 (2016).

88. Hanafusa, H., Torii, S., Yasunaga, T. & Nishida, E. Sprouty1 and Sprouty2 provide a control mechanism for the Ras/MAPK signalling pathway. *Nat. Cell Biol.* **4,** 850–858 (2002).

89. Yim, D. G. R., Ghosh, S., Guy, G. R. & Virshup, D. M. Casein kinase 1 regulates

Sprouty2 in FGF–ERK signaling. *Oncogene* **34,** 474–484 (2015).

90. Caunt, C. J. & Keyse, S. M. Dual-specificity MAP kinase phosphatases (MKPs): shaping the outcome of MAP kinase signalling. *FEBS J.* **280,** 489–504 (2013).

91. Todd, J. L., Tanner, K. G. & Denu, J. M. Extracellular regulated kinases (ERK) 1 and ERK2 are authentic substrates for the dual-specificity protein-tyrosine phosphatase VHR. A novel role in down-regulating the ERK pathway. *J. Biol. Chem.* **274,** 13271–80 (1999).

92. Glick, D., Barth, S. & Macleod, K. F. Autophagy: cellular and molecular mechanisms. *J. Pathol.* **221,** 3–12 (2010).

93. Hanada, T. *et al.* The Atg12-Atg5 conjugate has a novel E3-like activity for protein lipidation in autophagy. *J. Biol. Chem.* **282,** 37298–302 (2007).

94. Matsushita, M. *et al.* Structure of Atg5.Atg16, a complex essential for autophagy. *J. Biol. Chem.* **282,** 6763–72 (2007).

95. Miller, B. C. *et al.* The autophagy gene ATG5 plays an essential role in B lymphocyte development. *Autophagy* **4,** 309–314 (2008).

96. Pua, H. H., Dzhagalov, I., Chuck, M., Mizushima, N. & He, Y.-W. A critical role for the autophagy gene Atg5 in T cell survival and proliferation. *J. Exp. Med.* **204,** 25–31 (2007).

97. O'Sullivan, T. E. *et al.* Atg5 Is Essential for the Development and Survival of Innate Lymphocytes. *Cell Rep.* **15,** 1910–1919 (2016).

98. Lee, H. K. *et al.* In Vivo Requirement for Atg5 in Antigen Presentation by Dendritic Cells. *Immunity* **32,** 227–239 (2010).

99. Jounai, N. *et al.* The Atg5 Atg12 conjugate associates with innate antiviral immune responses. *Proc. Natl. Acad. Sci. U. S. A.* **104,** 14050–5 (2007).

100. Guo, H. *et al.* Atg5 Disassociates the V1V0-ATPase to Promote Exosome Production and Tumor Metastasis Independent of Canonical Macroautophagy. *Dev. Cell* **43,** 716–730.e7 (2017).

101. Ohno, S. & Kuroda, M. in 261–270 (Humana Press, New York, NY, 2016). doi:10.1007/978-1-4939-3753-0_19

102. Azmi, A. S., Bao, B. & Sarkar, F. H. Exosomes in cancer development, metastasis, and drug resistance: a comprehensive review. *Cancer Metastasis Rev.* **32,** 623–42 (2013).

103. Petrik, J. Immunomodulatory effects of exosomes produced by virus-infected cells. *Transfus. Apher. Sci.* **55,** 84–91 (2016).

104. Maxson, M. E. & Grinstein, S. The vacuolar-type H^+-ATPase at a glance - more than a proton pump. *J. Cell Sci.* **127,** 4987–93 (2014).

105. Palokangas, H., Metsikko, K. & Vaananen, K. Active Vacuolar H'ATPase Is Required for Both Endocytic and Exocytic Processes during Viral Infection of BHK-21 Cells*. **269,** 17577–17585 (1994).

106. Jeong, K., Kwon, H. Y., Jeong, M. S., Sohn, E. J. & Kim, S.-H. CNOT2 promotes degradation of p62/SQSTM1 as a negative regulator in ATG5 dependent autophagy. *Oncotarget* **8,** 46034–46046 (2017).

107. Malathi, K. *et al.* RNase L interacts with Filamin A to regulate actin dynamics and barrier function for viral entry. *MBio* **5,** e02012 (2014).

108. Irwin, C. R., Favis, N. A., Agopsowicz, K. C., Hitt, M. M. & Evans, D. H. Myxoma Virus Oncolytic Efficiency Can Be Enhanced Through Chemical or Genetic Disruption of the Actin Cytoskeleton. *PLoS One* **8,** e84134 (2013).

109. Arulanandam, R. *et al.* Microtubule disruption synergizes with oncolytic virotherapy by inhibiting interferon translation and potentiating bystander killing. *Nat. Commun.* **6,** 6410 (2015).

110. Friedrich, B. M. *et al.* A Functional Role for ADAM10 in Human Immunodeficiency Virus Type-1 Replication. *Retrovirology* **8,** 32 (2011).

111. Tacke, F., Liedtke, C., Bocklage, S., Manns, M. P. & Trautwein, C. CREB/PKA sensitive signalling pathways activate and maintain expression levels of the hepatitis B virus pre-S2/S promoter. *Gut* **54,** 1309–17 (2005).

112. Mahoney, D. J. *et al.* Virus-tumor interactome screen reveals ER stress response can reprogram resistant cancers for oncolytic virus-triggered caspase-2 cell death. *Cancer Cell* **20,** 443–56 (2011).

113. Otsubo, C. *et al.* TSPAN2 is involved in cell invasion and motility during lung cancer progression. *Cell Rep.* **7,** 527–38 (2014).

114. Yaseen, I. H., Monk, P. N. & Partridge, L. J. Tspan2: a tetraspanin protein involved in oligodendrogenesis and cancer metastasis. *Biochem. Soc. Trans.* **45,** 465–475 (2017).

115. Andreu, Z. & Yáñez-Mó, M. Tetraspanins in extracellular vesicle formation and function. *Front. Immunol.* **5,** 442 (2014).

116. Tavor, S. *et al.* CXCR4 regulates migration and development of human acute myelogenous leukemia stem cells in transplanted NOD/SCID mice. *Cancer Res.* **64,** 2817–24 (2004).

117. Singh, V., Erb, U. & Zöller, M. Cooperativity of CD44 and CD49d in leukemia cell homing, migration, and survival offers a means for therapeutic attack. *J. Immunol.* **191,** 5304–16 (2013).

118. Bailon, E. *et al.* Overexpression of progelatinase B/proMMP-9 affects migration regulatory pathways and impairs chronic lymphocytic leukemia cell homing to bone marrow and spleen. *J. Leukoc. Biol.* **96,** 185–199 (2014).

Contribution from collaborators

Dr. Larissa Pikor, Bell lab post-doctoral fellow, aided in experimental design and research plan as well as helped analyze deep sequencing data.

Adrian Pelin, Bell lab PhD student, helped analyze deep sequencing data.

John Chmara, research technician, helped maintain screen cells in culture during my absence.

Julia Petryk, Bell lab senior animal technician, performed intra-venous injections and harvested organs and bones for experiments.

Christiano Tanese de Souza, Auer lab senior animal technician, performed intra-venous and all subcutaneous injections as well as harvested organs and bones for experiments.

Fasteris SA in Switzerland performed Illumina deep sequencing of screen samples.

Appendix

Table 2. Screen PCR 2 primer sequences. In orange: TruSeq p5 (forward) or p7 (reverse) adapters, blue: stagger, purple: barcode sequences.

PCR 2 Primer	Sequence (5'-3')
Forward 1	AATGATACGGCGACCACCGA GATCTACACTCTTTCCCTACACGACGCTCTTCCGATCT T **AAGTAGAG** TCTTGTGGAAAGGACGAAACACCG
Forward 2	AATGATACGGCGACCACCGA GATCTACACTCTTTCCCTACACGACGCTCTTCCGATCT AT **ACACGATC** TCTTGTGGAAAGGACGAAACACCG
Forward 3	AATGATACGGCGACCACCGA GATCTACACTCTTTCCCTACACGACGCTCTTCCGATCT GAT **CGCGCGGT** TCTTGTGGAAAGGACGAAACACCG
Forward 4	AATGATACGGCGACCACCGA GATCTACACTCTTTCCCTACACGACGCTCTTCCGATCT CGAT **CATGATCG** TCTTGTGGAAAGGACGAAACACCG
Forward 5	AATGATACGGCGACCACCGA GATCTACACTCTTTCCCTACACGACGCTCTTCCGATCT TCGAT **CGTTACCA** TCTTGTGGAAAGGACGAAACACCG
Forward 6	AATGATACGGCGACCACCGA GATCTACACTCTTTCCCTACACGACGCTCTTCCGATCT ATCGAT **TCCTTGGT** TCTTGTGGAAAGGACGAAACACCG
Reverse 1	CAAGCAGAAGACGGCATACGAGAT **AAGTAGAG** GTGACTGGAGTTCAGACGTGTGCTCTTCCGATCT T TCTACTATTCTTTCCCCTGCACTGT
Reverse 2	CAAGCAGAAGACGGCATACGAGAT **ACACGATC** GTGACTGGAGTTCAGACGTGTGCTCTTCCGATCT AT TCTACTATTCTTTCCCCTGCACTGT
Reverse 3	CAAGCAGAAGACGGCATACGAGAT **CGCGCGGT** GTGACTGGAGTTCAGACGTGTGCTCTTCCGATCT GAT TCTACTATTCTTTCCCCTGCACTGT
Reverse 4	CAAGCAGAAGACGGCATACGAGAT **CATGATCG** GTGACTGGAGTTCAGACGTGTGCTCTTCCGATCT CGAT TCTACTATTCTTTCCCCTGCACTGT
Reverse 5	CAAGCAGAAGACGGCATACGAGAT **CGTTACCA** GTGACTGGAGTTCAGACGTGTGCTCTTCCGATCT CGATC TCTACTATTCTTTCCCCTGCACTGT
Reverse 6	CAAGCAGAAGACGGCATACGAGAT **TCCTTGGT** GTGACTGGAGTTCAGACGTGTGCTCTTCCGATCT T TCTACTATTCTTTCCCCTGCACTGT

Curriculum Vitae

Education

2018-2022 Graduate-entry Medicine | University College Dublin

- Dublin, Ireland

2016-2018 Master of Science in Biochemistry | University of Ottawa

- Department of Biochemistry, Microbiology and Immunology
- Ottawa Hospital Research Institute
- **Graduate thesis**: Identifying mechanisms of resistance to oncolytic virotherapy in acute leukemia through a genome-wide CRISPR screen
- Co-supervisors: Dr. Natasha Kekre and Dr. John Bell

2012-2016 Bachelor of Science in Biomedical Science | University of Ottawa

- Summa cum laude, Faculty of Science
- Ottawa Hospital Research Institute
- **Honours thesis**: Tailored oncolytic viral therapeutics for pancreatic cancer
- Supervisor: Dr. John Bell and Dr. Carolina Ilkow (Post-doctoral fellow)

Research

2016-2018 Centre for Innovative Cancer Research

- Ottawa Hospital Research Institute
- Graduate studies with Department of BMI, Faculty of Medicine, University of Ottawa,
- Identified novel mechanisms of resistance to oncolytic virotherapy using a genome-wide CRISPR screen
- Co-supervisors: Dr. Natasha Kekre and Dr. John Bell

2015-2016 Centre for Innovative Cancer Research

- Ottawa Hospital Research Institute
- Undergraduate honours thesis with Faculty of Science, University of Ottawa,
- Investigated the *in vitro* effects of an engineered oncolytic rhabdovirus
- Supervisor: Dr. John Bell and Dr. Carolina Ilkow (Post-doctoral fellow)

2014 Biophysics

- Department of Physics, Faculty of Science, University of Ottawa
- NSERC-USRA undergraduate
- Collected proteins for manipulation and study of protein patterns

- Supervisor: Dr. James Harden

2013-2014 Centre for Innovative Cancer Research

- Ottawa Hospital Research Institute
- Undergraduate Research Opportunity Program (UROP), Faculty of Science, University of Ottawa
- Live cell imaging, cloning of fusion proteins and transformation for study in mammalian cells
- Supervisor: Dr. Douglas A. Gray

Awards & Scholarships

2017-2018 Graduate admission scholarship ($15,000)
University of Ottawa

2016-2017 Queen Elizabeth II Graduate Scholarship in Science and Technology ($15,000)
University of Ottawa

2016-2017 Excellence Scholarship ($8,100)
University of Ottawa

2012-2016 Undergraduate admission scholarship ($4,000 annually)
University of Ottawa

2012-2016 Dean's honour list
University of Ottawa

2015 OHRI Summer student research seminar: Bronze
Ottawa Hospital Research Institute

2014 NSERC-USRA ($6,000)
University of Ottawa

2013-2014 Undergraduate Research Opportunity Program ($1,000)
University of Ottawa

Publications

Jennings V, Wedge M-E, Boileau M, Laight B, **Rose E**, Cote M-L, Bellamy D, Tanese de Souza C, Petryk J, Alkayyal A, Surendran A, Jacobs E, Auer R, Gibbings D, Melcher A, Bell JC, and Ilkow CS. Enhancing oncolytic virotherapy by exosome-

mediated microRNA reprogramming of the tumour microenvironment [manuscript in preparation]. 2018.

Rose E, Pikor L, Bell JC, Kekre N. Identifying mechanisms of resistance to oncolytic virotherapy in acute leukemia through a genome-wide CRISPR screen [abstract]. In: Ottawa Blood Disease Centre: Trainee Research Symposium; 2017 May 4; Ottawa, ON.

Poster presentations

Rose E, Pikor L, Bell JC, Kekre N. Identifying mechanisms of resistance to oncolytic virotherapy in acute leukemia through a genome-wide CRISPR screen. Poster session presented at: 4th Canadian Cancer Research Conference; 2017 Nov 5-7; Vancouver, BC.

Rose E, Pikor L, Bell JC, Kekre N. Identifying mechanisms of resistance to oncolytic virotherapy in acute leukemia through a genome-wide CRISPR screen. Poster session presented at: 2nd annual Summit for Cancer Immunotherapy; 2017 Jun 25-28; Gatineau, QC.

Rose E, Kennedy M, Auer R, Atkins H, Kekre N, Bell JC. Optimization of an infected cell vaccine for the treatment of acute leukemia. Poster session presented at: 16th annual OHRI Research Day; 2016 Nov 15; Ottawa, ON.

Rose E, Ilkow CS, Boileau M, Gibbings D, Bell JC. Tailored oncolytic viral therapeutics for pancreatic cancer. Poster session presented at: Summit for Cancer Immunotherapy. 9th annual Canadian Cancer Immunotherapy Consortium (CCIC) Symposium; 2016 Jun 26-29; Halifax, NS.

Volunteer experience

2016-2018 **Let's Talk Science**, Ottawa

2016 **Connecting Young Minds Research Conference**, Ottawa

2015 **Canadian Blood Services In-clinic**, Ottawa